https://doi.org/10.1093/plcell/koad224 THE PLANT CELL 2023: 1–18

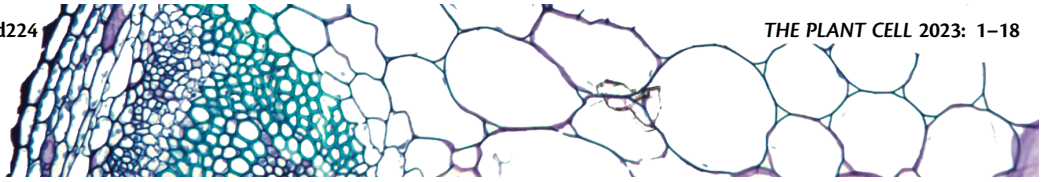

Research Article

Pathogen-induced m^{6}A dynamics affect plant immunity

Wil Prall [1,†] Arsheed H. Sheikh [2,†] Jeremie Bazin [3] Jean Bigeard [3] Marilia Almeida-Trapp [2] Martin Crespi [3,*] Heribert Hirt [2,4,*] and Brian D. Gregory [1,*]

1 Department of Biology, University of Pennsylvania, Philadelphia, PA 19104, USA
2 Center for Desert Agriculture, King Abdullah University of Science and Technology, Thuwal 23955-6900, Saudi Arabia
3 CNRS, INRA, Institute of Plant Sciences Paris-Saclay IPS2, Universite Paris Sud, Universite Evry, Universite Paris-Diderot, Sorbonne Paris-Cite, Universite Paris-Saclay, 91190 Gif-sur-Yvette, France
4 Max F. Perutz Laboratories, University of Vienna, 1030 Vienna, Austria

*Author for correspondence: bdgregor@sas.upenn.edu (B.D.G.), martin.crespi@universite-paris-saclay.fr (M.C.), heribert.hirt@kaust.edu.sa (H.H.)
†These authors contributed equally.
The author responsible for distribution of materials integral to the findings presented in this article in accordance with the policy described in the Instructions for Authors (https://academic.oup.com/plcell/) is: Brian D. Gregory (bdgregor@sas.upenn.edu).

Abstract

Posttranscriptional regulation of mRNA mediated by methylation at the N^6 position of adenine (N^6-methyladenosine [m^{6}A]) has profound effects on transcriptome regulation in plants. Focused studies across eukaryotes offer glimpses into the processes governed by m^{6}A throughout developmental and disease states. However, we lack an understanding of the dynamics and the regulatory potential of m^{6}A during biotic stress in plants. Here, we provide a comprehensive look into the effects of m^{6}A on both the short-term and long-term responses to pathogen signaling in *Arabidopsis* (*Arabidopsis thaliana*). We demonstrate that m^{6}A-deficient plants are more resistant to bacterial and fungal pathogen infections and have altered immune responses. Furthermore, m^{6}A deposition is specifically coordinated on transcripts involved in defense and immunity prior to and proceeding the pathogen signal flagellin. Consequently, the dynamic modulation of m^{6}A on specific stress-responsive transcripts is correlated with changes in abundance and cleavage of these transcripts. Overall, we show that the m^{6}A methylome is regulated prior to and during simulated and active pathogen stress and functions in the coordination and balancing of normal growth and pathogen responses.

Introduction

Plants respond to their environment through a constant balancing act, mitigating action, and reaction to harmful and beneficial stimuli. In the innate immune response specifically, *Arabidopsis* (*Arabidopsis thaliana*) can detect and respond to bacterial and fungal proteins through recognition of conserved pathogen/microbe-associated molecular patterns (PAMPs/MAMPs) thereby initiating PAMP/MAMP-triggered immunity (PTI/MTI) (Jones and Dangl 2006). For example, a well-characterized PAMP of *Pseudomonas* is flagellin (flg22), which triggers downstream signaling responses including reactive oxygen species (ROS) production, activation of mitogen-activated protein kinases (MAPKs), and activation of defense genes characteristic of a PTI response (Jones and Takemoto 2004; Denoux et al. 2008; Bigeard et al. 2015). Upon activation, PTI changes plant defense hormone profiles (i.e. salicylic acid [SA] and jasmonic acid [JA]) to optimize the immune response toward specific pathogens and reprogram normal development (Felix et al. 1999; Zhang et al. 2010; Berens et al. 2017). Such coordination in response to pathogen infection requires complex regulation on multiple tiers of gene expression (Schenk et al. 2000; Birkenbihl et al. 2017; Li et al. 2019).

More recently, it has been shown that posttranscriptional regulatory mechanisms, such as RNA modifications, are major

Received January 26, 2022. Accepted July 18, 2023. Advance access publication August 23, 2023

IN A NUTSHELL

Background: To determine how plants respond to bacterial and fungal pathogens, researchers are interested in analyzing the transcriptome, the global collection of RNAs in eukaryotic cells to see how plants react. Not only changes in individual RNA copy number (abundance) but also significant changes in the covalent additions to specific nucleotides in messenger RNAs (mRNAs) (i.e. nucleotide modification) are observed. In this work, we investigate the addition of a methyl group onto the mRNA nucleotide adenosine (N^6-methyladenosine [m^6A]). m^6A addition to mRNA is of great interest because its presence in individual mRNAs is known to affect RNA stability, translation, and maturation.

Question: What is the m^6A transcriptomic landscape before and after exposure to simulated and real pathogen infection in *Arabidopsis*? How does global reduction in m^6A across all mRNAs affect plant preparedness and reactivity to pathogen stress?

Findings: Global depletion of m^6A in mutant and transgenic seedlings and adult *Arabidopsis* plants (*mta* mutant and *35S:ALKBH10B* overexpressor) results in increased resistance to bacterial and fungal infections, altering fundamental plant immune response. m^6A deposition is specifically coordinated on RNA transcripts directly involved in defense and immunity prior to and following pathogen signaling and stress. The modulation of m^6A on specific transcripts is correlated with changes in abundance and internal mRNA cleavage demonstrating this modification as another layer of control before and during the immune response.

Next Steps: The m^6A modification is added to transcripts by "writer" proteins, removed by "erasers," and bound by "readers." Understanding how these proteins are regulated themselves and how they regulate the selective addition and removal of these marks in the context of pathogen infection is of critical importance.

regulators of cellular gene expression during stress responses (Floris et al. 2009; Anders et al. 2018; Anderson et al. 2018; Bazin et al. 2018; Engel et al. 2018; Rigo et al. 2019; Wilkinson et al. 2021; Govindan et al. 2022). N^6-methyladenosine (m^6A) is the most prevalent internal covalent mRNA modification currently known in eukaryotic transcriptomes and has been shown to influence transcript fate and function (Dominissini et al. 2012; Meyer et al. 2012; Wang, Lu, et al. 2014; Wang et al. 2015; Wang, Li, et al. 2014; Zhao et al. 2017; Prall et al. 2023; Sharma et al. 2023). The primary m^6A writer complex in *Arabidopsis* consists of METHYLTRANSFERASE A (MTA), METHYLTRANSFERASE B (MTB), FKBP INTERACTING PROTEIN 37 (FIP37), and VIRILIZER (VIR), accompanied by other cofactors which all have highly conserved mammalian orthologs (METTL3, METTL14, and Wilms tumor 1-associated protein) (Roundtree and He 2016; Reichel et al. 2019). Deficiency in these proteins can result in altered m^6A deposition and subsequent gene expression causing infertility, developmental defects, and cellular and organismal death in both plant and animal systems (Bodi et al. 2012; Batista et al. 2014; Schwartz et al. 2014; Haussmann et al. 2016; Yoon et al. 2017). m^6A marks are directly recognized and bound by reader proteins that contain methyl-binding aromatic pockets (YTH domains). Due to their highly conserved C-termini that contain the YTH domains, the reader proteins are named EVOLUTIONARILY CONSERVED C-TERMINAL REGION (ECT) in *Arabidopsis* and have been shown to have important functions in plant development (Arribas-Hernández et al. 2018; Scutenaire et al. 2018). Likewise, m^6A can be removed from mRNAs by both active demethylases (erasers including ALKB and ALKB-Homology (ALKBH) family proteins) and by passive "dilution" (multiple rounds of RNA decay and transcription). Two out of 5 *Arabidopsis* ALKBH proteins have been shown to be physiologically relevant during development by directly affecting the stability of transcripts involved in floral transition and most recently in biomass and yield (Duan et al. 2017; Yu et al. 2021) and in response to viral and pathogen infection (Martínez-Pérez et al. 2017; Li et al. 2018; Zhang, Zhuang, et al. 2021; Zhang, Wang, et al. 2021). However, our understanding of the functional significance of m^6A in the context of plant biotic stress responses remains largely understudied.

The biological role of m^6A on mRNAs has been studied in more detail recently. It has been shown that m^6A exerts multiple effects on transcript fate, notably destabilizing effects with examples in zebrafish (Zhao et al. 2017), *Drosophila* (Haussmann et al. 2016), mouse (Zheng et al. 2013), and human cells (Wang, Lu, et al. 2014), positively (Mao et al. 2019) and negatively (Choi et al. 2016; Slobodin et al. 2017) impacting translation in bacterial and human cells, and in plants, influencing alternative polyadenylation (Farhat et al. 2021), noncoding RNA maturation (Bhat et al. 2020), and translation (Luo et al. 2020; Govindan et al. 2022; Guo et al. 2022). In *Arabidopsis*, global analysis of mRNA stability in plants deficient in the m^6A writer MTA (*mta ABI3:MTA;* hereafter referred to as *mta*) indicated that m^6A deposition has a stabilizing capacity in adult leaf tissue (Anderson et al. 2018). Investigation across plant species has shown both negative and positive impacts on transcript fate and maturation (Duan et al. 2017; Wei et al. 2018; Zhou et al. 2019; Bhat et al. 2020; Parker et al. 2020; Shao et al. 2021; Guo et al. 2022),

with 1 study in strawberry (*Fragaria vesca*) supporting a location- and context-specific model of m^{6}A function in plants (Zhou et al. 2021). Here, we assessed the dynamic and multifaceted role of m^{6}A during the pathogen defense response in plants. Based on the finding that deficiency in m^{6}A resulted in an altered transcriptomic response and an increase in resistance to challenge by both simulated and virulent abiotic stressors, we used a combination of transcriptome-wide and phenotypic analyses to provide evidence for a potent role for m^{6}A in dynamically modulating transcript abundance and stability during the pathogen infection process in plants.

Results

m^{6}A function modulates plant immune responses and immunity to pathogen infection

In an effort to understand the role of m^{6}A in the posttranscriptional regulation of the plant immune response to pathogen infections, we took advantage of *Arabidopsis* lines known to be deficient in m^{6}A methylation including *mta* (*ABI3:MTA*), carrying a T-DNA insertion in the major methyltransferase that has its embryonic development defects rescued by expressing *MTA* with the embryo-specific *ABI3* promoter (Bodi et al. 2012) and 2 T-DNA insertion lines: *fip37-4* (SALK_018636), which contains an insertion in intron 7 of *FIP37* (AT3G54170) and was previously described as a weak allele (Růžička et al. 2017), and *vir-2* (SALK_014875), which contains an insertion in exon 19 of *VIRILIZER* (*VIR*, AT3G05680) and acts as a weak allele of this genotype, both of which are components of the m^{6}A methyltransferase complex (Supplemental Fig. S1A). We detected transcripts upstream of both insertions and significantly less downstream of each insertion, suggesting comparable amounts of truncated *FIP37* and *VIR* as well as small amounts of full-length transcript being produced in these lines (Supplemental Fig. S1B). We also added into our analyses an overexpressing line (*35S:ALKBH10B*) of the most abundant m^{6}A erasing protein ALKBH10B (AT4G02940) and a rescue complementation line of *mta*, p*MTA:MTA-YFP*. To assess the relative difference in total m^{6}A on mRNA, we performed m^{6}A dot blot analyses comparing levels in polyA$^+$-selected RNA of the *35S:ALKB10B*, *fip37-4*, and *vir-2* lines described above compared to Col-0 and the established *mta* mutant line. We observed the greatest decrease in global m^{6}A in *mta* as expected and considerable decrease in all other lines relative to Col-0 (Supplemental Fig. S1C). To assess their response to pathogen stress, we challenged *mta*, *35S:ALKBH10B*, *fip37-4*, and *vir-2* with *Pseudomonas syringae* DC3000 (*Pst* DC3000). Compared to Col-0, we observed significantly less bacterial multiplication in *mta*, *fip37-4*, *vir-2*, and *35S:ALKBH10B* (Fig. 1, A and B; Supplemental Fig. S1D). Relatedly, we could reverse this enhanced immunity phenotype conferred by m^{6}A deficiency in the p*MTA:MTA-YFP* rescue line as we observed no changes in bacterial load compared to wild type, suggesting a specific role of m^{6}A machinery in proper bacterial immunity (Fig. 1A; Supplemental Fig. S1D). An additional pathovar of *P. syringae*, pv. *maculicola* ES4326 (*Psm* ES4326), and a fungal pathogen, *Botrytis cinerea*, were also tested on *mta* mutant plants. We observed more efficiently restricted infection of both additional pathogens (Fig. 1, B and C), like the results for *P. syringae* (Fig. 1A). Overall, these results reveal a role for the m^{6}A writing and erasing machinery in the global response to pathogen infection.

To further examine the effects that a global decrease in m^{6}A has on basal immune responses, we measured several flg22-induced early and late PTI readouts in *mta* and *35S:ALKBH10B* genotypes. For late PTI readouts, we observed a notable difference in response to long-term flg22 growth inhibition in both *mta* and *35S:ALKBH10B*. More specifically, we observed a significant difference in response to flg22 in both root growth and total seedling weight in both m^{6}A-deficient genotypes compared to in Col-0 (Fig. 1D; Supplemental Fig. S1E). This was most notable for the *35S:ALKBH10B*, which had similar root growth and total seedling weight before and after flg22 treatment compared with Col-0 (Fig. 1D; Supplemental Fig. S1E), suggesting that m^{6}A hypomethylation affects late PTI responses in plants. Measuring callose deposition, we observed a significant increase in deposition in *mta* plants compared to Col-0 after flg22 treatment (Fig. 1F). For early PTI readouts, we measured ROS bursts and found that *mta* plants show a sharp peak of flg22-induced production that decreases at a faster rate than that in Col-0 (Fig. 1E). Additionally, the activation of the MPK3, 4, and 6 were elevated in *mta* mutants compared to in Col-0 after flg22 elicitation (Supplemental Fig. S1F). Finally, we measured defense-related hormones SA and JA along with the antimicrobial compound camalexin (CA) as key components to an optimized immune response (Berens et al. 2017; Zhou et al. 2019). We observed a significant increase in quantified SA, JA, and CA levels in *mta* after *Pst* DC300 challenge (Fig. 1, G to I). In total, these results indicate that deficiency in m^{6}A through perturbation of the methyltransferase complex or overexpression of a major eraser enzyme significantly affects basal immune responses in plants, likely through m^{6}A-mediated regulation of the transcriptome.

m^{6}A abundance affects immune-related mRNA profile before and after pathogen exposure

To further investigate the immunity phenotypes observed in m^{6}A-depleted genotypes, we analyzed the flg22-triggered transcriptomic response in 14-d-old Col-0, *mta*, and *35S:ALKBH10B* plants, as well as the *Pst* DC3000-triggered transcriptomic response in 4-wk-old Col-0 and *mta* plants. RNA sequencing (RNA-seq) identified ~4,000 to 6,500 transcripts differentially regulated in flg22-treated seedlings of both m^{6}A-depleted genotypes (Fig. 2, A to D; Supplemental Data Set S1), and ~2,400 to 3,200 in *Pst* DC3000-treated *mta* adult plants (Supplemental Fig. S2, A to D, and Data Set S1). Next, we overlapped the differentially

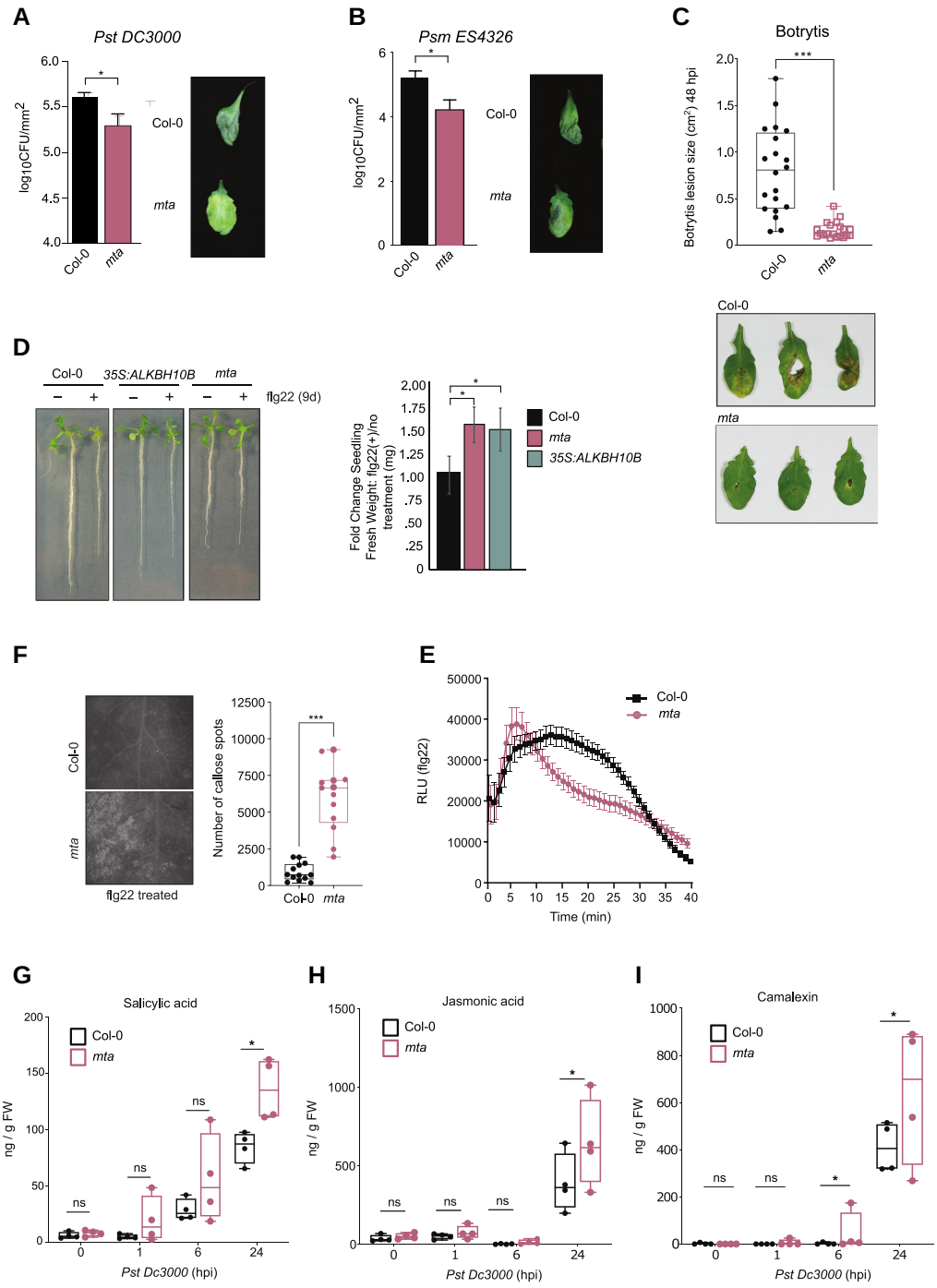

Figure 1. Effects of global m^{6}A levels on immune response. **A)** Bacterial count in Col-0 and *mta* plants infected with PstDC3000. Leaves were syringe infiltrated with 10^6 CFU/mL of bacteria and bacterial count was determined at 2 dpi. Results are represented as mean ± SEM ($n = 3$). Asterisks indicate statistical differences according to Student's *t*-test, * denotes $P < 0.05$. **B)** *Psm* ES4326 multiplication measured 2 dpi in Col-0 and *mta*. Results are shown as mean ± SEM ($n = 3$). Asterisks indicate statistical differences according to Student's *t*-test, * denotes $P < 0.05$. **C)** *B. cinerea* lesions in Col-0 and *mta*. Four-week-old plants were drop inoculated with 5×10^6 spores/mL suspension, and lesion size was measured at 72 hpi. Box plot center line, median; box limits, upper and lower quartiles; whiskers, 1.5× interquartile range; and points, outliers. Results are mean ± SEM. *** denotes $P < 0.001$, 2-tailed *t*-test. **D)** Growth inhibition of Col-0 and *mta* seedlings grown with 1 μM concentration of flg22 peptide for 9 d. Results are mean ± SEM ($n = 24$), * denotes $P < 0.05$, 2-tailed *t*-test. **E)** flg22-induced callose deposition. Col-0 and *mta* leaves were treated with 1 μM flg22 for 24 h. Box plot center line, median; box limits, upper and lower quartiles; whiskers, 1.5× interquartile range; and points, outliers. Results are mean ± SEM. *** denotes $P < 0.001$, 2-tailed *t*-test. **F)** ROS burst in *Arabidopsis* Col-0 and *mta* leaf discs triggered by 1 μM flg22. The data are shown as means ± SEM from 12 leaf discs. **G to I)** SA **G)**, JA **H)**, and CA **I)** quantification in Col-0 and *mta* plants is shown as ng/g of fresh weight. The data are shown as means ± SEM from 4 replicates. * represents $P < 0.05$ when *mta* was compared with data from Col-0 plants, 2-tailed *t*-test. Box plot center line, median; box limits, upper and lower quartiles; whiskers, 1.5× interquartile range; and points, outliers. Results are mean ± SEM.

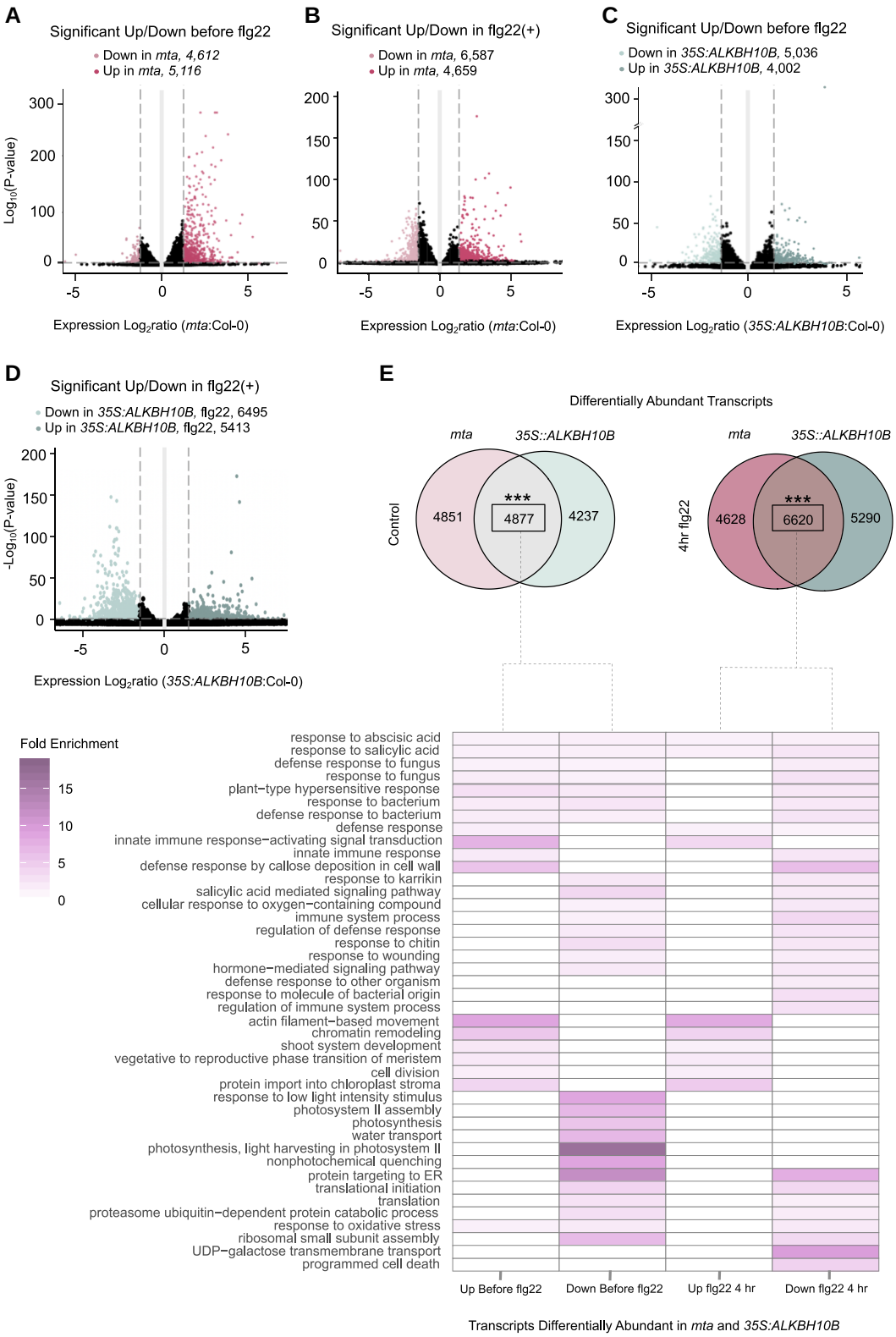

Figure 2. Transcriptome profile during pathogen stress in m^{6}A-depleted backgrounds. **A to D)** Volcano plots of differentially expressed RNA transcripts from mRNA-seq in 14-d-old seedlings using DeSeq2 (2.0 FC, FDR $P_{adj} < 0.05$) in **A)** *mta* before treatment, **B)** *mta* 4-h flg22 treatment, **C)** *35S:ALKBH10B* before treatment, and **D)** *35S:ALKBH10B* 4-h flg22 treatment. **E)** Overlap of significantly differential transcripts in both m^{6}A-depleted backgrounds before and after flg22 treatment. *** represents $P < 0.001$ for enrichment in the overlap, hypergeometric test used. GO analysis enrichment represented as fold enrichment for transcripts significantly up or down in each overlap with corresponding *P*-values of <0.05 compared against background of all detectable transcripts.

abundant transcripts in *mta* and *35S:ALKBH10B*, revealing 4,877 and 6,620 transcripts significantly up- or downregulated in both m^{6}A depletion backgrounds before and after flg22 exposure, respectively (Fig. 2E; Supplemental Data Set S1). Interestingly, we observed a significant enrichment for transcripts involved in defense response in these m^{6}A-depleted backgrounds prior to any biotic stress perturbation (Fig. 2E). After flg22 exposure, transcripts involved in stress and fundamental cellular processes were also differentially regulated (Fig. 2E). The same trend was observed in adult plants in the m^{6}A-depleted *mta* background; there was significant enrichment of defense transcripts prior to any exposure, confirming a transcriptomic "priming" to defense in m^{6}A-depleted backgrounds and an altered response following exposure (Supplemental Fig. S2E). Comparing the distribution of fold change in these m^{6}A-affected transcripts revealed an overall negative shift in fold change in seedlings, providing further evidence of m^{6}A acting as a stabilizing mark in plants (Anderson et al. 2018; Parker et al. 2020) (Supplemental Fig. S2, F and G).

m^{6}A deposition is regulated on immune transcripts before and after pathogen exposure

We evaluated the m^{6}A methylation profile before and after pathogenic challenge to further interpret the transcriptome and whole plant phenotypes. We performed m^{6}A-seq (Dominissini et al. 2013) in 14-d-old Col-0, *mta*, and *35S:ALKBH10B* seedlings before and after flg22 treatment, as well as before and after PstDC3000 treatment in 4-wk-old Col-0 and *mta* plants. The libraries were prepared with 3 biological replicates and resulted in 8 to 10 million uniquely mapped reads across conditions. The MACS2 peak-calling algorithm was used to identify peaks using a false discovery rate (FDR) < 0.01, and high-confidence peaks were determined to be those present in all 3 replicates for each genotype and condition. We identified ~9,300 to 13,000 peaks across all conditions corresponding to ~7,500 to 9,400 transcripts (Fig. 3A; Supplemental Fig. S3, A to D). We observed a decrease in total peak number in the *mta* and *35S:ALKBH10B* backgrounds as expected, reporting 2,271 to 2,919 hypomethylated (loss of detectable m^{6}A high-confidence peaks) peaks in *mta* and *35S:ALKBH10B* across conditions (Fig. 3A; Supplemental Data Set S2). The distribution of m^{6}A predominated in the 3′ UTR of transcripts with detectable enrichment after the start codon and across the coding region (CDS) (Fig. 3B). Gene ontology (GO) analysis revealed distinct functional profiles of m^{6}A harboring transcripts before and after flg22 and PstDC3000 treatment (Supplemental Fig. S4, A to C). High-confidence sequence motifs were identified across all conditions within m^{6}A peaks: the highly conserved RRACH (R = A/G; H = A/C/U) sequence was enriched in seedlings before and after treatment, UGUA in flg22-treated seedlings, and RRACH in untreated and treated adult tissue (Supplemental Fig. S5). Interestingly, we observed a decrease in peak enrichment in the 3′ UTR and an inverse increase near the start codon in seedlings following flg22 treatment, while the opposite trend was observed for *Pst* DC3000-treated adult plants (Fig. 3, C and D; Supplemental Fig. S4A). This could suggest a possible condition- and developmental-specific m^{6}A accumulation switching in plant transcriptomes in response to biotic stressors. Continuing, we identified the hypomethylated peaks in both *mta* and *35S:ALKBH10B* seedlings before and after flg22 treatment, revealing 731 and 493 high-confidence MTA and ALKBH10B targets, respectively (Fig. 3E; Supplemental Data Set S2). GO enrichment revealed a striking polarization in these hypomethylated populations, with a significant fold enrichment for immune and defense-related transcripts prior to flg22 exposure and enrichment for development, growth, and cellular processes after treatment (Fig. 3F; Supplemental Data Set S2) suggesting that in response to pathogen signaling, m^{6}A deposition is specifically enriched in transcripts related to the defense and growth trade-off. We then assessed if this was also occurring in adult tissue by comparing seedling- and adult-specific hypomethylated transcripts and confirmed a shared and adult-specific defense and immune m^{6}A profile prior to any pathogenic exposure. In total, these results suggest that m^{6}A is involved in posttranscriptionally regulating the trade-off between pathogen and growth responses during biotic stress responses.

Next, in order to obtain transcripts with decreased m^{6}A levels in m^{6}A-deficient backgrounds, we utilized the m^{6}A site differential algorithm within the exomePeak package with slight modification and a >1.5-fold cutoff as performed previously (Meng et al. 2013; Zhou et al. 2021) to compare changes in m^{6}A peak enrichment between samples. We identified 293 and 152 transcripts with significantly decreased m^{6}A levels in both *mta* and *35S:ALKBH10B* seedlings before and after flg22, respectively, and 646 in *mta* adult plants before treatment (Supplemental Fig. S6, A to C, and Data Set S2). In agreement with the hypomethylation analysis, we observed enrichment for defense and immune transcripts before flg22 and PstDC3000 treatment in seedling and adult tissue, confirming a distinct immune-related m^{6}A profile which is significantly altered in m^{6}A-deficient genotypes (Supplemental Fig. S6, A to C).

5′ mRNA cleavage sites are enriched in m^{6}A peaks and less abundant in m^{6}A-containing transcripts following flg22 treatment

Previous work has described a relationship between m^{6}A and transcript stability. To test this, we performed genome-wide mapping of uncapped and cleaved transcripts (GMUCT) (Willmann et al. 2014). The GMUCT method captures cleaved and degradation intermediates through specific adapter ligation to the 5′end of RNAs with a free 5′-monophosphate (Vandivier et al. 2015; Anderson et al. 2018; Yu et al. 2021). Using the high-confidence hypomethylated transcripts and transcripts with 1.5 fold change (FC) decrease in m^{6}A intensity in the m^{6}A-deficient backgrounds, we calculated the percent enrichment of 5′end cleavage

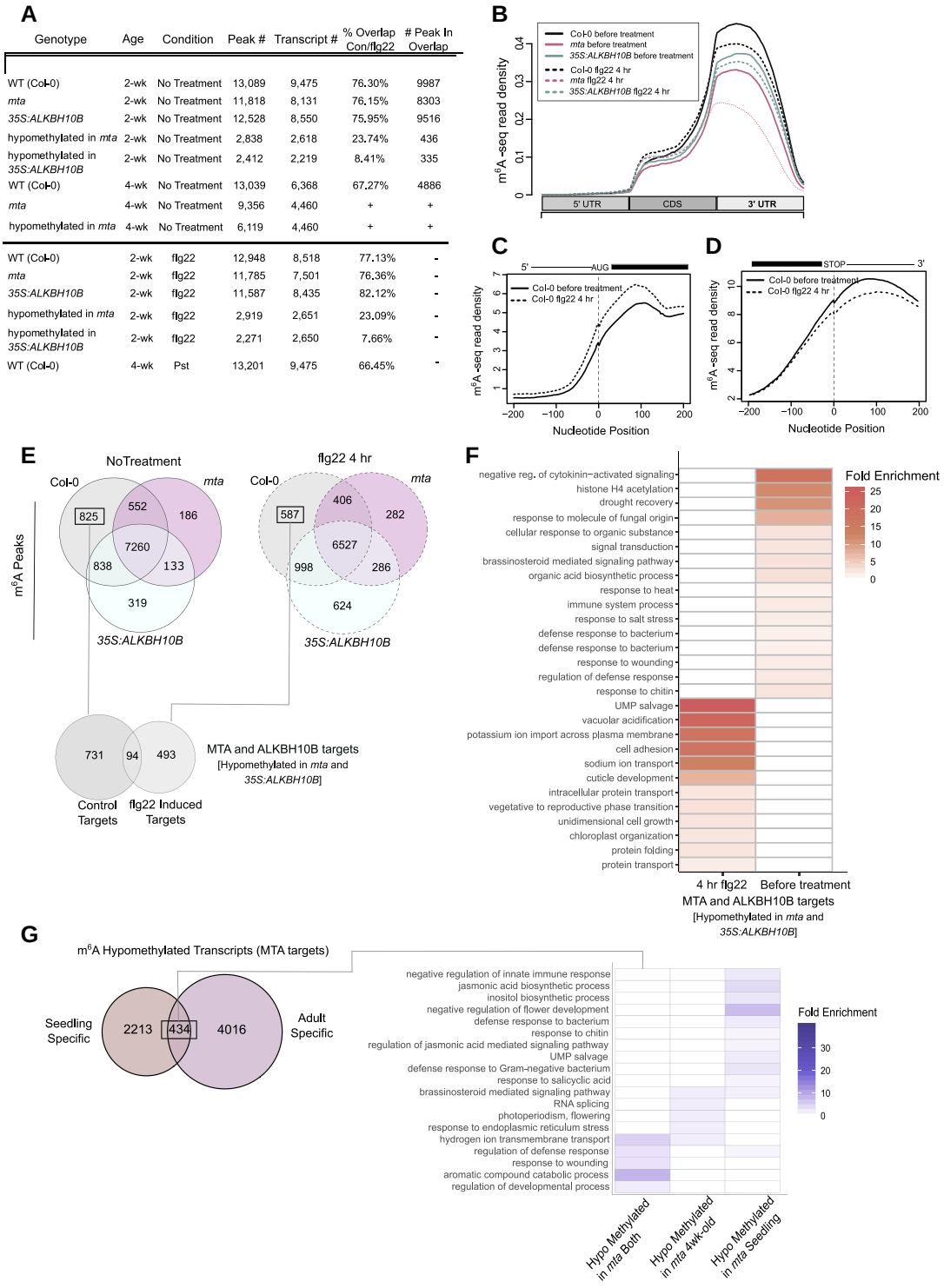

Genotype	Age	Condition	Peak #	Transcript #	% Overlap Con/flg22	# Peak In Overlap
WT (Col-0)	2-wk	No Treatment	13,089	9,475	76.30%	9987
mta	2-wk	No Treatment	11,818	8,131	76.15%	8303
35S:ALKBH10B	2-wk	No Treatment	12,528	8,550	75.95%	9516
hypomethylated in *mta*	2-wk	No Treatment	2,838	2,618	23.74%	436
hypomethylated in *35S:ALKBH10B*	2-wk	No Treatment	2,412	2,219	8.41%	335
WT (Col-0)	4-wk	No Treatment	13,039	6,368	67.27%	4886
mta	4-wk	No Treatment	9,356	4,460	+	+
hypomethylated in *mta*	4-wk	No Treatment	6,119	4,460	+	+
WT (Col-0)	2-wk	flg22	12,948	8,518	77.13%	-
mta	2-wk	flg22	11,785	7,501	76.36%	-
35S:ALKBH10B	2-wk	flg22	11,587	8,435	82.12%	-
hypomethylated in *mta*	2-wk	flg22	2,919	2,651	23.09%	-
hypomethylated in *35S:ALKBH10B*	2-wk	flg22	2,271	2,650	7.66%	-
WT (Col-0)	4-wk	Pst	13,201	9,475	66.45%	-

Figure 3. m^{6}A profile during pathogen stress. **A)** Summary table of m^{6}A sequencing results and MACS2 high confidence called peaks with FDR < 0.0 (+) indicates sequencing was not performed, and (−) is replicate data in table. **B)** Average stacked localization of high-confidence m^{6}A peaks before and after treatment, 14-d-old seedlings in Col-0, *mta*, and *35S:ALKBH10B* genotypes. **C, D)** Average stacked localization of m6A-RIP-seq read density in the ±200 bp surrounding START **C)** and STOP **D)** codons, Col-0 visualized. **E)** Overlap of high-confidence m^{6}A peaks before and after and flg22 treatment in seedlings between Col-0, *mta*, and *35S:ALKBH10B*. Highlighted peaks represent hypomethylated transcripts in both m^{6}A-deficient genotypes in each condition and were used to generate **F)**. **F)** GO enrichment represented as heat map, $P < 0.05$ against background of all m^{6}A containing transcripts. Hypomethylated transcripts found in both *mta* and *35S:ALKBH10B* represented before and after flg22 treatment. **G)** Overlap of seedling- and adult-specific hypomethylated transcripts in *mta* before treatment. GO analysis enrichment represented as fold enrichment for transcripts significantly up- or downregulated in each overlap with corresponding *P*-values of <0.05 compared against background of all detectable transcripts.

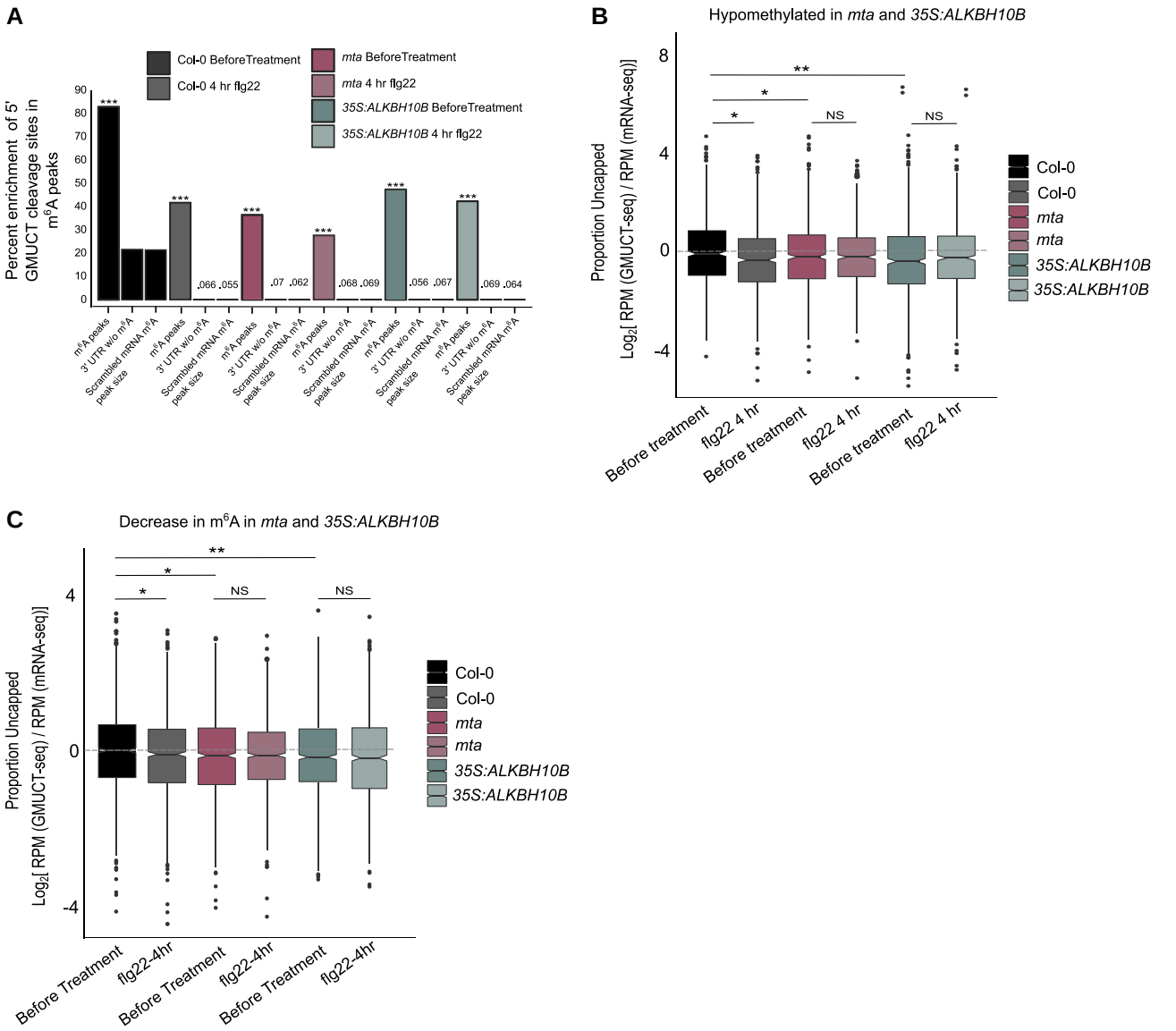

Figure 4. Transcript stability of m^{6}A containing RNAs during flg22 treatment. **A)** Percent enrichment of 5′ GMUCT cleavage sites within m^{6}A peaks in 14-d-old Col-0, *mta*, and *35S:ALKBH10B* seedlings. Transcripts with complete loss or significant reduction in m^{6}A-deficient backgrounds were used, percent enrichment compared to random peaks generated from 3′ UTRs containing no m^{6}A, and random peaks generated from entire mRNA. *** represents $P < 0.001$ for enrichment in the overlap between m^{6}A peaks and GMUCT 5′end reads, hypergeometric test used. **B, C)** Average proportion uncapped (GMUCT RPM normalized to RNA-seq RPM for each mRNA) for **B)** transcripts hypomethylated in *mta* and *35S:ALKBH10B* representing MTA ALKBH10B high-confidence targets OR **C)** transcripts with significant reduction in m^{6}A intensity. Boxplot center line, median; box limits, upper and lower quartiles; whiskers, 1.5× interquartile. Points represent outliers. Statistical significance determined through Wilcoxon ranked sum test, 3 replicates per genotype/condition. * and ** denote $P < 0.05$ and 0.01, respectively.

within these m^{6}A peaks. We observed significant enrichment of GMUCT 5′ cleavage sites in m^{6}A peaks in Col-0 plants, while a reduction in *mta* and *35S:ALKBH10B*-deficient backgrounds was identified as expected. Interestingly, we also found a reduction in m^{6}A-regulated cleavage in flg22-treated plants across all genotypes (Fig. 4A). These data provide further evidence that m^{6}A likely inhibits local ribonucleolytic cleavage, as previously described (Anderson et al. 2018). Furthermore, the overall reduction of m^{6}A peaks in flg22-treated tissue (Fig. 3, A to C) suggests a coordination of m^{6}A reduction or removal in response to pathogen signaling. We then calculated the relative stability of mRNAs using the proportion uncapped metric for each expressed transcript as performed previously (Vandivier et al. 2015; Anderson et al. 2018). Using the high-confidence MTA and ALKBH10B targets from above, we did not observe an average bias in GMUCT stability before flg22 treatment in this population (Fig. 4, B and C; Supplemental Data Set S3). However, we did observe a significant increase in average transcript stability following flg22 treatment in Col-0 for both groups of transcripts, while this trend was no

longer significant or reversed in both hypomethylation backgrounds (Fig. 4, B and C; Supplemental Data Set S3). These results imply that the flg22-induced changes in stability are lost with global m^{6}A reduction, further suggesting a direct connection between m^{6}A and stability of these mRNAs.

Region- and condition-specific reductions in m^{6}A correlate with differential mRNA abundance

To determine whether the loss of m^{6}A has a significant impact on transcript abundance, we compared the mRNA-seq reads from transcripts containing m^{6}A peaks (peaks lost in *mta* and *35S:ALKBH10B*), as defined above, before and after treatment. We confidently determined which transcripts have a significant change in mRNA abundance when they lose or have a significant reduction in m^{6}A, before and after treatment (Supplemental Fig. S7, A and B, and Data Set S2). We observed a relatively small population of transcripts when using these criteria: 69 and 74 transcripts with decreased m^{6}A and a measured decrease and increase in abundance before treatment, respectively (Supplemental Fig. S7A), and 111 and 33 transcripts with the same pattern after flg22 treatment (Supplemental Fig. S7B). We performed GO analysis on these transcripts which have m^{6}A-dependent mRNA abundance profiles. Before any treatment, we found enrichment for defense response transcripts in the increasing mRNA abundance population, suggesting loss of m^{6}A contributes to their increased abundance prior to pathogen perturbation (Supplemental Fig. S7A). Of interest were transcripts encoding PECTIN METHYLESTRERASE 17 (PME17), known to be directly involved in resistance to *B. cinerea* (Penninckx et al. 1998; Bethke et al. 2014; Del Corpo et al. 2020), and PAMP-INDUCED COILED COIL (PICC), a regulatory protein involved in pathogen-induced callose deposition and plant immunity through interaction with the PAMP-mediated induction of callose synthase POWDERY MILDEW RESISTANT 4 (PMR4) (Nishimura et al. 2003; Wang et al. 2019) (Supplemental Data Sets S1 to S3). Alternatively, the transcript-encoding ZINC-FINGER PROTEIN1 (ZF1), which functions as a transcriptional repressor involved in the inhibition of growth under stress, was found to be positively regulated by m^{6}A (i.e. decreased in the m^{6}A-deficient pool) (Kodaira et al. 2011; Xie et al. 2019). Analysis in flg22-treated samples revealed increased enrichment for immune and defense transcripts in the population with decreased abundance after loss of m^{6}A (Supplemental Fig. S7B). We highlight transcripts encoding RNA polymerase II C-terminal domain CTD phosphatase-like-3 (CPL3), a negative regulator of immune gene expression (Li et al. 2014); SMALL PHYTOCYTOKINES REGULATING DEFENSE AND WATER LOSS (SCREW), which functions as an immunomodulatory phytocytokine-relaying immune signaling (Liu et al. 2022); and VASCULAR ASSOCIATED DEATH1 (VAD1), a protein involved in the regulation of defense and cell death in response to pathogens (Lorrain et al. 2004; Khafif et al. 2017) in this group.

Additionally, in the population of transcripts with an increase in mRNA and decreased m^{6}A in *mta* and *35S:ALKBH10B* after flg22 treatment, we found the transcript-encoding WRKY46, a known interactor of NONEXPRESSER OF PR GENES1 (NPR1) (Zhang, Zhu, et al. 2021), which is a key regulator of SA-mediated systemic acquired resistance (Myers et al. 2023), and OVERLY TOLERANT TO SALT2 (OTS2), a deSUMOylating enzyme involved in modulating SA signaling stress responses (Supplemental Data Sets S1 to S3). We observed the same trend in adult tissue, confirming an enrichment for transcripts with decreased m^{6}A and increased mRNA abundance involved in defense response and immunity before infection conditions (Supplemental Fig. S7C and Data Sets S1 and S2). We then asked if there were any specific signatures within these mRNA subpopulations that may explain their differential abundance. We did not find any subpopulation-specific m^{6}A peaks or patterns. However, we identified an enrichment of a GAAAG motif in the increasing population only (Supplemental Fig. S8A). We also observed significantly more m^{6}A signal present along the CDS in the population of mRNAs with decreasing abundance in the hypomethylation backgrounds, which is not present in the population with increasing abundance (Fig. 5, A to D). It is notable that there was no significant difference in the 3′ UTR m^{6}A levels between the 2 populations in Col-0 before and after flg22 treatment (Fig. 5, A to D). We also observed a massive reduction of m^{6}A signal in the 3′ UTR in *mta* as compared to Col-0 specifically in the subpopulation of transcripts with increased mRNA abundance in the hypomethylation backgrounds (Fig. 5, A to D). Assessing the cumulative distribution of FC in these populations revealed a population of m^{6}A-deficient transcripts with decreased levels prior to pathogen stimulation in both seedling and adult tissue, as well as a population with increased abundance in agreement with previous studies (Fig. 5, E and F) (Anderson et al. 2018; Parker et al. 2020). Interestingly, we observed a major shift after flg22 treatment revealing a cumulative distribution of transcripts biased toward decreasing abundance in m^{6}A-deficient backgrounds, suggesting a shift toward m^{6}A stabilizing transcripts during flg22 treatment specifically (Fig. 5E). Overall, our results reveal a target transcript stabilizing effect for m^{6}A specifically in the context of plant pathogen signaling.

m^{6}A has an established connection with modulating transcript stability. We thus sought to determine how individual transcript stability changes in both m^{6}A-deficient backgrounds focused on genes with established functions in the response to pathogens. To test the influence of each m^{6}A-deficient background on individual transcript stability, before and after pathogen stress, we assessed the relative degradation rates of transcripts encoding proteins involved in the coordinated defense response. Following vacuum infiltration with the transcriptional inhibitor cordycepin, we compared transcript abundance over time before and after flg22 treatment. We highlight *VAD1*, *CPL3*, *SCREW3*, and *ZF1* as examples of transcripts encoding proteins involved

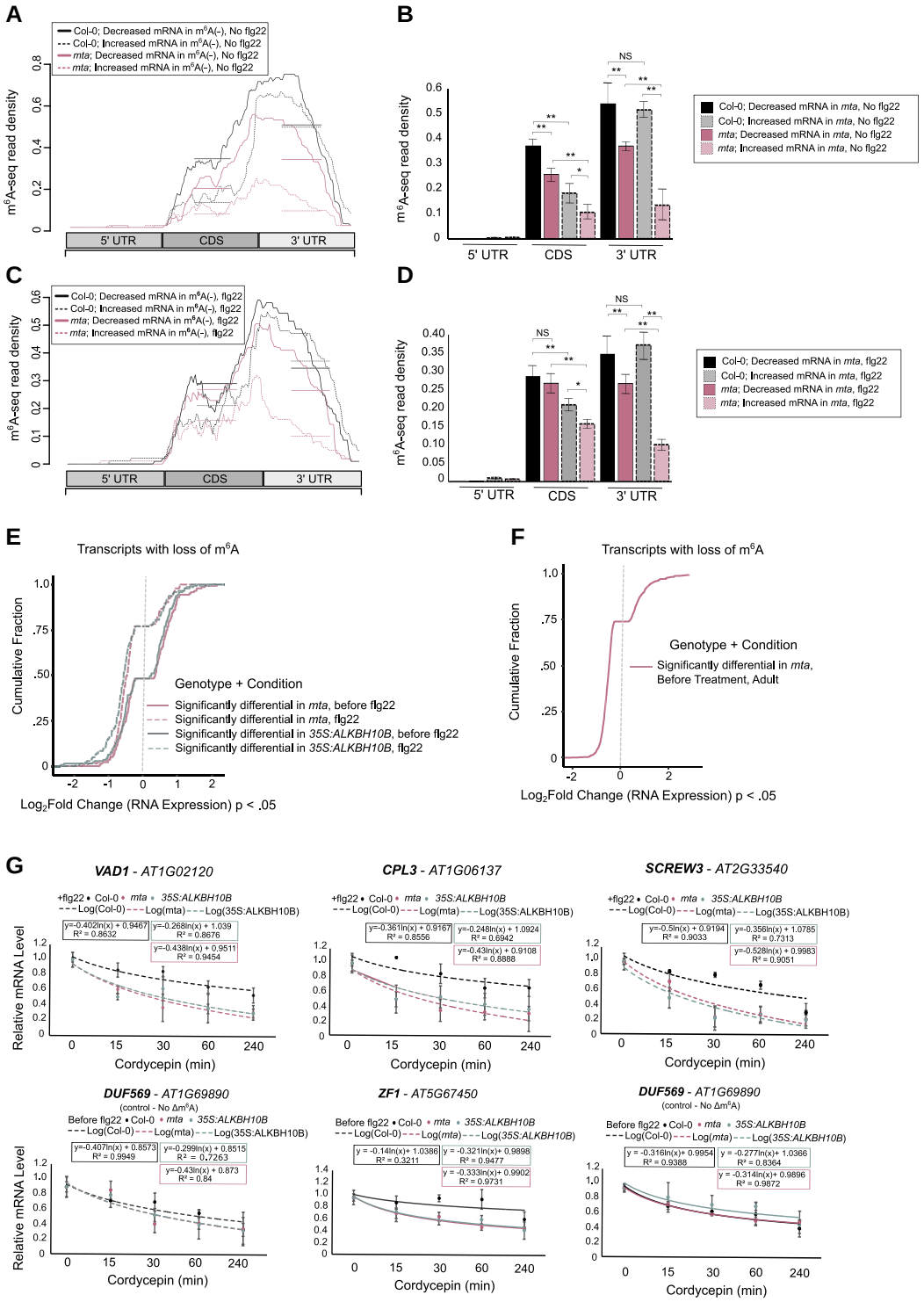

Figure 5. Condition and developmental m^{6}A signatures. **A to D)** Average stacked localization of transcripts with decreased m^{6}A and significant FC in mRNA abundance in m^{6}A-depleted backgrounds. 14-d-old seedlings before and after flg22 treatment, Col-0 (black), *mta* (red), increasing abundance (dotted), and decreasing abundance (solid). **A)** Distribution before treatment **B)** Quantification of average sequencing read density in **A)**. **C)** Distribution after 4-h flg22 treatment. **D)** Quantification of C. Statistical significance determined by Wilcoxon ranked sum test and 1-tailed t-test; * and ** denote $P < 0.05$ and 0.01, respectively; error bars calculated as standard error. **E)** Cumulative distribution of transcript FC for transcripts with loss of m^{6}A in *mta* and *35S:ALKBH10B* before and after 4-h flg22 treatment. **F)** Cumulative distribution of transcript FC for transcripts with loss of m^{6}A in *mta* and significant change in transcript abundance *mta*/Col-0 in adult tissue after as compared to before infection. **G)** mRNA stability assay for *VAD1*, *CPL3*, *SCREW3*, and *ZF1* mRNAs in *mta* and *35S:ALKBH10B* m^{6}A-deficient backgrounds as compared to Col-0. Total RNA extractions following cordycepin treatment and RT-qPCR at indicated time points. *MUSE7* mRNA was utilized as an internal control, *DUF569* was chosen as a m^{6}A negative control. Error bars calculated as standard error.

in the defense response that were negatively impacted in m^{6}A-deficient backgrounds (faster degradation) (Fig. 5G), validating a stabilizing role of m^{6}A on these RNAs. Additional analysis of other transcripts encoding proteins involved in the pathogen response before and after flg22 treatment in *mta* and *35S:ALKBH10B* m^{6}A-deficient backgrounds revealed similar trends but not as strong as those highlighted in Fig. 5G (Supplemental Fig. S8B). These data validate that loss of m^{6}A can negatively impact transcript stability in 2 independent genetic backgrounds.

Taken together, these findings suggest that many m^{6}A targets linked to biotic stress can be positively and negatively influenced by loss of m^{6}A before and after stress. We hypothesize that these observed differences are not only a result of changes in deposition but also of condition and developmental differences in the growing number of known m^{6}A interactors and complexes recognizing, binding, and removing these marks during both stress and development.

Discussion

As with other RNA maturation and modification processes, the addition of m^{6}A has the capability to influence many aspects of the transcript life cycle. Despite recent progress, we still lack a complete understanding of the scope and potential of the most abundant internal mRNA modification, specifically the selectivity and dynamic nature of this mark during plant immunity responses. It has been shown that both the deposition and interpretation of m^{6}A are significantly reprogrammed during short- and long-term stress response (Martínez-Pérez et al. 2017; Anderson et al. 2018; Engel et al. 2018; Li et al. 2018; Alvarado-Marchena et al. 2021; Tian et al. 2021; Yang et al. 2021; Zhang, Wang, et al. 2021; Govindan et al. 2022; Mao et al. 2022; Wang et al. 2022). Our study demonstrates and broadens this understanding of m^{6}A in the posttranscriptional regulation of the plant transcriptome in response to pathogen stress. We describe a role of m^{6}A in regulating and reprogramming the transcriptome in the context of the immune response both before the pathogen signal is detected and following immediate and long-term pathogen infection. We demonstrate that depletion of m^{6}A positively alters the response to simulated and virulent pathogen exposure (Fig. 1). These data present a complex paradigm, whereby m^{6}A plays a regulatory role in both the short- and long-term response to PAMP and pathogen signals. Furthermore, we observed heightened levels of SA, JA, and CA following infection, suggesting that either or both hormone sensing and signaling networks are altered in the context of RNA hypomethylation plant genotypes (Fig. 1).

Comparing the transcriptomic profiles before and after pathogen stress in m^{6}A-depleted mutants revealed enrichment of m^{6}A occurrence for key defense and immunity transcripts prior to any exposure. Thus, m^{6}A-deficient plants were observed to be in a "primed" hyperactive status in both seedling and adult tissue before pathogen or elicitor exposure, followed by further alteration in the immune response by pathogen or immune elicitation (Fig. 2). The m^{6}A epitranscriptome in these conditions revealed a distinct polarization, whereby transcripts involved in immunity and defense were hypomethylated in the m^{6}A-deficient backgrounds before treatment and growth and development transcripts hypomethylated after pathogen signaling (Fig. 3). This suggests a distinct m^{6}A signature on defense-related transcripts under normal conditions that is altered in the m^{6}A-deficient backgrounds and contributes to the phenotypes we observe. These findings corroborate with previous studies on the stress and developmental-specific m^{6}A signatures in mRNAs (Anderson et al. 2018; Zhou et al. 2021; Govindan et al. 2022; Wang et al. 2022). Degradome analysis filtering with these transcripts revealed significant enrichment of cleavage sites within m^{6}A peaks and revealed a significant correlation between transcript stability and m^{6}A presence after but not prior to pathogen stress (Figs. 4 and 5). Furthermore, we highlight transcripts with significant depletion in m^{6}A and corresponding changes in mRNA abundance across all conditions. Interestingly, we revealed subpopulations of transcripts, whereby loss of m^{6}A differentially regulated their abundance (Fig. 5) as shown before (Zhou et al. 2021). We observed significant enrichment of m^{6}A in the CDS of transcripts with decreasing abundance in the RNA methylation-deficient backgrounds suggesting that the m^{6}A location along the mRNA may also influence transcript abundance and stability (Fig. 5). Furthermore, global shifts in total abundance of m^{6}A-depleted transcripts in m^{6}A-deficient backgrounds prior to and during stress and in seedlings and adults revealed that m^{6}A has stabilizing effects that are likely condition- and or development-dependent influences on transcript fate. More specifically, both the m^{6}A profile and correlation to transcript abundance and stability changed in each condition (Figs. 3 to 5). Our data agree with previous findings (Anderson et al. 2018; Parker et al. 2020) that demonstrate bias of m^{6}A to positively influence transcript stability and abundance in the *Arabidopsis* transcriptome. Interestingly, we expand on this showing a dramatic global shift during flg22 treatment, whereby most transcripts that lost m^{6}A signal had significantly decreased abundance compared to Col-0, implying an increased potency of m^{6}A on these transcripts in a condition-specific manner (Figs. 2 to 5). Importantly, we used 2 m^{6}A-deficient backgrounds to determine hypomethylated transcripts with significant mRNA level changes. We determined with high confidence which transcripts are directly and significantly altered in m^{6}A-deficient mutants prior to and proceeding pathogen stress and validated changes in stability for selected candidates. Our analysis revealed a list of high-confidence transcripts involved in balancing the plant defense response influenced both directly and indirectly by the m^{6}A mark.

In total, we describe a transcriptome regulatory role for m^{6}A in plant immunity in *Arabidopsis*, showing that plant defense is orchestrated by a complex regulation of posttranscriptional m^{6}A modification of specific sets of mRNAs in the

plant transcriptome. We show the m^6A methylome is carefully regulated prior to and during simulated and active pathogen stress to coordinate normal growth and pathogen responses. In total, our findings provide evidence that further studies focusing on the coordinated deposition, removal, and interpretation of the m^6A mark are necessary to fully understand its functions during biotic as well as abiotic plant stress responses.

Materials and methods

Plant material and treatments

The *Arabidopsis* (*A. thaliana*) genotypes used were ecotype Col-0, *mta ABI3:MTA (mta)* (Bodi et al. 2012), *virilizer-2* (*vir-2*, SALK_014875), and *fip37-4* (SALK_018636) (Růžička et al. 2017). Mutant lines were obtained from ABRC, homozygocity was confirmed, and primers are listed in Supplemental Data Set S4. Transcript abundance from the mutant loci in these lines was determined through reverse transcription quantitative PCR (RT-qPCR) as described below relative to Col-0. The MTA complementation line was generated by agrobacterium-mediated transformation of *mta* plants by the MTA genomic locus cloned into the pGWB440 vector. The overexpression line *35S:ALKBH10B* was generated by transforming plasmids into *alkbh10b-1* (SALK_00421C), described previously (Duan et al. 2017). For flg22 and stability assays, seeds were surface-sterilized and stratified at 4 °C for 3 to 5 d. Seedlings were then grown for 14 d in vitro in large Petri dishes containing 0.5× MS Basal Salts (Sigma #M6899), 0.5% sucrose (Euromedex 200-301-B) v/v, 0.5% agar Type E (Sigma #A4675) w/v, and 0.05% MES pH 5.7 (Sigma #M8250) v/v, in the following conditions: 16-h light/8-h dark, average lighting of 120 μmol/m^2/s, 20 °C day/18 °C night, 60% hygrometry. One day before treatment, a liquid medium (same medium without agar) was added to the plates under sterile conditions, and plates were transferred onto the bench. Seedlings were treated with a final concentration of 1 μM flg22 for 0 (no treatment) or 240 min. Seedlings were finally harvested, rapidly dried with paper, flash-frozen in liquid nitrogen, and stored at −80 °C.

Generation of transgenic plants

For the construction of *35S:ALKBH10B*, full-length cDNA was obtained from ABRC. The GreenGate hierarchical cloning system was used (Lampropoulos et al. 2013; Engler et al. 2014). Briefly, all Type II restriction sites were removed, and full-length *ALKBH10B* cDNA was cloned into Level −1. *35S:ALKBH10B* was constructed using GreenGate toolkit supplied by Addgene. All parts were assembled into the pAGM4723 binary vector, including the red seed fluorescent expression cassette as a selectable seed marker. Transformation was performed using the floral dip method (Zhang et al. 2006). All primers used are included in Supplemental Data Set S4. For the generation of the *MTA* complementation line, the genomic locus of *MTA* (AT4G10760) was cloned into the gateway-compatible pDONR207 vector and later transferred to the pGWB440 binary vector. The plasmid harboring the construct was transformed into *Agrobacterium* GV3101 competent cells. Later, *mta* mutant plants were transformed with the construct using the floral dip method as described.

Growth inhibition assays

For assaying long-term flg22 responses, 5-d-old seedlings, grown on MS agar plates, were transferred to liquid media for 24 h. A final concentration of 1 μM flg22 peptide was added, and plants were grown as mentioned above with light shaking for 9 d. Thereafter, seedling weight was measured.

Pathogen infection assays

P. syringae tomato DC3000 and *P. syringae maculicola* ES4326 strains (Dong et al. 1991; Xin and He 2013) were grown on King's B agar plates with 50-μg/mL rifampicin at 28 °C. Bacteria were collected in 10 mM $MgCl_2$. Twelve 4-wk-old plant leaves were infiltrated with bacteria at a concentration of 10^6 cfu/mL using a needleless syringe. Bacteria were released from 3 leaf discs (4 mm) in 500 μL of 10 mM $MgCl_2$ with 0.01% Silwet 77 v/v by incubating at 28 °C at 1,000 × *g* for 1 h. Serial dilutions were plated on LB medium with appropriate antibiotics. After incubation at 28 °C, bacterial colonies were counted. The experiment was repeated 3× with similar results. *B. cinerea* infection was performed as described in (Rayapuram et al. 2021). Briefly, 4-wk-old plants were inoculated with *B. cinerea* (strain: B05.10) by placing a 5 μL droplet of a spore suspension (5×10^5 spores/mL) on each rosette leaf (3 fully expanded leaves per plant). Trays were covered by a transparent plastic lid to maintain high humidity. Lesion diameter was measured after 72 h of infection using ImageJ analysis tool.

ROS production assay

ROS burst was determined by a luminol-based assay as described with modifications (Ranf et al. 2011). Twelve leaf discs (4 mm) were incubated overnight in a white 96-well plate with 100 μL of H_2O to reduce the wounding effect. The next day, 100 μL of reaction solution containing 50 μM of luminol (Sigma) and 10 μg/mL of horseradish peroxidase (Sigma) supplemented with 1 μM of flg22. The measurement was conducted immediately after adding the solution with a luminometer (GloMax, Promega), for a period of 40 min with a 1 min reading interval between readings. The measurements were indicated as means of Relative Light Units (RLU). The experiments were repeated 3× with similar results.

MAPK activation assays

Col-0 and *mta* seedlings were grown on ½ MS-agar plates. After 14 d, seedlings were transferred to liquid ½ MS overnight to eliminate stress. The ½ MS was replaced with fresh ½ MS supplemented with 1 μM of flg22 and harvested at indicated time points. Proteins were extracted using extraction buffer. The frozen seedlings were homogenized in 100 μL of extraction buffer (150 mM Tris-HCl, pH 7.5, 150 mM NaCl, 5 mM EDTA, 2 mM EGTA, 10 mM DTT, 10 mM Na_2MoO_4,

1 mM $NaVO_3$, 10 mM NaF, 10 mM β-glycerol phosphate, 0.5 mM phenylmethylsulfonyl fluoride, and 1% proteinase inhibitor cocktail v/v [Sigma]). After centrifugation at 13,000 × *g* for 20 min at 4 °C, the protein concentration of the supernatants was determined using a Bradford assay. Thirty micrograms of protein was separated on a 10% polyacrylamide gel and transferred on a PVDF membrane. After overnight blocking with TBST-5% milk, the membrane was washed 3× with TBST. Immunoblot analysis was performed using antiphospho-p44/42 MAPK (1:5,000; Cell Signaling Technology) for 2 h as primary antibody and peroxidase-conjugated goat antirabbit antibody (1:10,000; Promega) for 1 h with 5 10-min washes in between the incubations. The experiment was repeated twice with similar results.

Callose deposition

Callose deposition was conducted as described by (Wang et al. 2021) with modifications. Briefly, 4-wk-old Col-0 and *mta* mutant plants were infiltrated with 1 μM of flg22. After 24 h, 12 excised leaves from each genotype were destained in ethanol:acetic acid solution (3:1) for 3 to 4 h. Samples were washed with 150 mM K_2HPO_4 for 30 min. Cleared leaves were stained with 0.01% aniline blue v/v (Sigma) in 150 mM K_2HPO_4 (pH = 9.5) overnight in the dark with constant shaking. Callose deposits were visualized under a DAPI filter using a fluorescence microscope. Callose deposits were counted using ImageJ software. The experiment was repeated 2× with similar results.

SA and CA measurement

The extraction of phytohormones (SA and CA) was performed according to (Almeida Trapp et al. 2014) using a solution of 80% methanol in water containing 10 ng/mL of d5-IAA as an internal standard. The compounds were quantified by HPLC-ESI-SRM in a Thermo Fisher TQS-Altis Triple Quadrupole Mass Spectrometer coupled to a Thermo Scientific Vanquish MD HPLC system. The chromatographic separation was carried out in a UPLC column (Agilent Eclipse Plus C18, RRHD, 1.8 μm, 2.1 × 50 mm), and the compounds were eluted using water (A) and acetonitrile (B) as the mobile phase at 0.6 mL/min and in a gradient elution mode as follows: 10% B for 0.5 min, 10% to 55% B at 4.5 min, 55% to 100% B at 4.7 min, 100% until 6.0 min, and 100% to 10% B at 6.1% and 10% until 8 min. The column was kept at 55 °C. The statistical analyses were perfumed in R studio (V. 1.2.5033). When needed, the data were transformed to achieve a normal distribution of the residues, and the statistical significance from 3 replicates was evaluated by ANOVA followed by a Tukey test (Tukey HSD).

RNA isolation (mRNA-, m6A-, RIP-, and GMUCT-seq–qPCR)

RNA was extracted from whole seedlings (flg22-treated) using liquid N_2 homogenization. QIAzol-resuspended samples were heated to 45 °C and then further homogenized using Omni Tips (OMNI, Kennesaw GA, USA). RNA isolation was performed using QIAGEN miRNeasy mini columns (QIAGEN, Valencia, CA, USA), as detailed in the manufacturer's protocol. RNA was treated with RNase-free DNase (QIAGEN, Valencia, CA, USA) for 30 min and ethanol precipitated. RNA isolation from adult plants after PstDC3000 infection was performed using a NucleoSpin RNA plant kit (Macherey-Nagel, #740949) as per the manufacturer's instructions.

PolyA$^+$ mRNA selection (mRNA-, m6A-, RIP-, and GMUCT-seq)

PolyA$^+$ mRNA was selected using Dynabeads oligo dT beads from a Dynabeads mRNA direct purification kit (Thermo Fisher, Waltham, MA, USA). Purification was performed as described in the manufacturer's protocol using 2 selection rounds per batch of beads. PolyA-selected RNA was used for RNA-seq, GMUCT-seq, and input for m^{6}A-RNA immunoprecipitation sequencing (m^{6}A-RIP-seq).

RNA-seq

RNA-seq of flg22-treated samples from 14-d-old *mta*, *35S:ALKBH10B*, and Col-0 seedlings was performed with 3 biological replicates. RNA was extracted as detailed above, and eukaryotic RNA-seq with library preparation and sequencing (20 million raw reads) was performed using Illumina paired-end sequencing at Novogene (CA, USA). RNA quality from Col-0 and *mta* adult plants was validated by Bioanalyzer and quantified using a Qubit RNA Assay kit. RNA-seq was conducted using the Illumina TruSeq standard mRNA Library Preparation protocol as per the manufacturer's instructions for 50-bp paired-end sequencing. Three biological replicates were sequenced per condition.

m^{6}A-RIP-seq

m^{6}A-RIP-seq was performed using 3 μg of polyA$^+$-selected mRNA (from above) per replicate for 3 biological replicates of *mta*, *35S:ALKBH10B*, and Col-0, before and after flg22. Immunoprecipitation was performed as described previously (Anderson et al. 2018) with the following changes. RNA was heated at 75 °C for 5 min and immediately placed on ice for 2 min. The volume was brought to 660 μL for all samples with nuclease-free water. Then, 10-μL RNaseOUT (Life Technologies; Carlsbad, CA, USA), 200-μL 5× IP buffer (250 mM Tris-HCl, 750 mM NaCl, 0.5% v/v Igepal [CA-6300]), and 40 μL of 1 μg/μL m^{6}A antibody (202003, SYSY, Goettingen, Germany) were added to each sample, and samples were rotated at 4 °C for 2 h. While the samples and antibody mixture were rotating, Protein A beads (Dynabeads Protein A, Thermo Fisher Scientific, Waltham, MA, USA) were washed twice with 1-mL 1× IP buffer and resuspended in 1-mL 1× IP buffer containing 0.5-mg/mL BSA and rotated for 2 h at 4 °C. RNA antibody mixture was then cross-linked 2× with 0.15-Jcm^{-2} UV light (254 nm) in a Stratalinker. Meanwhile, Protein A beads were washed 2× in 1-mL 1× IP buffer, resuspended in 250 μL of 1× IP buffer,

and combined with RNA antibody solution. The mixture was incubated for 2 h at 4 °C. Beads were pelleted using a magnetic stand, and the supernatant was removed and stored at −80 °C as the unbound supernatant. Associated RNA was removed from beads by adding 95-μL proteinase K buffer (5 mM Tris pH 7.5, 1 mM EDTA, 0.25% SDS) supplemented with 5 μL of proteinase K and incubated for 45 min at 50 °C. The supernatant was removed as the m^6A^+ fraction. Beads were washed 2× with 300-μL 1× IP buffer and saved as m^6A^+ fractions. RNA was precipitated using glycogen, 3 M NaOAc, and 3× v/v 100% ethanol at −80 °C. The resulting RNA samples were prepared into libraries using the strand-specific RNA-seq protocol Illumina TruSeq standard mRNA Library Preparation and sent to Novogene (CA, USA) for 20 million paired-end reads per sample sequencing.

GMUCT sequencing

GMUCT libraries were constructed using polyA$^+$ RNA that was isolated as described above from 14-d-old seedlings, *mta*, and Col-0. Three biological replicates were prepared and sequenced for all samples used in this study as previously described (Willmann et al. 2014). GMUCT libraries were sequenced by Novogene (CA, USA) giving 20 million paired-end reads per sample.

Transcriptional arrest time course

mRNA degradation analysis was performed as previously described in Sorenson et al. (2018) with the following modifications. Four-day-old seedlings were grown as described above in the Plant material and treatments section and transferred to 1-mL liquid media in 24-well Petri dish plates with aeration (swirling 150 × *g*) for 24 h for acclimatization to liquid media. For flg22-treated samples, wells were spiked with 1 μM flg22 with continued shaking for 240 min. Before and following flg22 treatment, fresh liquid media supplemented with 1 mM cordycepin was introduced. Initial T_0 samples were frozen in liquid nitrogen. Vacuum infiltration was conducted 3×. Following the third release, tissue (10 seedlings per replicate) was collected at 15, 30, 60, and 240 min and immediately frozen and stored at −80 °C for RNA extraction.

RT-qPCR analysis

Total RNA was extracted from seedlings as described above. RNA (1 μg) was used for reverse transcription reactions using Maxima H Minus Reverse Transcriptase (Thermo Fisher). Resulting cDNA was amplified using a LightCycler 480 thermocycler (45 cycles, 60 °C). All experiments were done in biological triplicates with 2 technical replicates per biological replicate. Relative expression was normalized to *MUSE7* mRNA (AT5G466020) for decay experiments, as determined in Sorenson et al. (2018), which showed delayed decay rates during cordycepin treatment. *MUSE7* also did not display any alternative m^6A profiles or expression profiles across conditions. *ACTIN* mRNA was used to normalize RT analysis of T-DNA insertion mutants. Relative quantification of transcription was performed using the $C_T 2^{-\Delta CT}$ method, and final values are reported relative to T_0 to indicate decay over time. All primers used are listed in Supplemental Data Set S4.

Dot blot analysis

PolyA$^+$-selected mRNA (50, 150, and 300 ng) from 14-d-old seedlings was spotted on a SensiBlot plus Nylon membrane (Fermentas #M1002) and air-dried for 5 min. The membrane was UV cross-linked using a Stratalinker and blocked with PBST-5% milk for 3 h. The membrane was incubated overnight with m^6A antibody (Abcam#15320, 1:3500), washed, and subsequently incubated with goat antirabbit-HRP (Promega, 1:10000). The membrane was developed using Immobilon Forte Western HRP substrate (Millipore #WBLUFO500).

Analysis and quantification

Sequencing read analysis (mRNA-, m^6A-RIP-, and GMUCT-seq)

Reads from all RNA-seq were trimmed of adaptors using Cutadapt (version 1.9.1 using parameters -e 0.06 -O 6 -m 14) (Martin 2011). Trimmed sequence reads were collapsed to unique reads and first mapped to rRNA and repetitive regions in the TAIR10 reference genome using STAR (version 2.4.0; Dobin and Gingeras 2015), and the remaining reads were then mapped to the TAIR10 *Arabidopsis* reference genome using STAR with parameters—bamRemoveDuplicatesType UniqueIdentical. Subsequent read counts were calculated by HTSeq-count.

Differential abundance analysis (mRNA-seq)

To determine significant differences in transcript counts, differential abundance was calculated using featureCounts with default parameters from aligned RNA-seq read (Liao et al. 2014). Significant differential abundance was determined using the R package DESeq2 pairwise analysis (Love et al. 2014) for all replicates of *mta*, *35S:ALKBH10B*, and Col-0 with and without flg22 and PstDC3000 treatments. Gene functional ontology (GO enrichment) was performed using DAVID tools set at default parameters (Huang da et al. 2009). Background genes for each GO enrichment analysis were set to all transcripts detected across all conditions with read counts ≥10, as determined through featureCounts.

Identification of m^6A peaks and data analysis

In order to identify transcripts from our m^6A-seq experiments, which show statistical significant enrichment for m^6A, m^6A peaks were called using MACS2 as first detailed in (Dominissini et al. 2012). MACS2 was used to call peaks using significant cutoff of <5e−2. Peaks were called against the $m^6A(-)$ fraction (supernatant of m^6A pull down), and transcripts enriched in IP pull down as compared to the supernatant fraction were deemed m^6A peaks as in (Anderson et al. 2018). In brief, MACS2 was run under the following parameters -nomodel, -extsize 50, -p5e-2, -g32542107, with -g being set to approximately half the genome size to account for input files either + or − strandedness. Peaks were called against $m^6A(-)$ fraction. Transcripts enriched

for m^{6}A peaks in all replicates and with higher abundance mRNA (reads per million [RPM] > 10) were utilized for subsequent analysis and deemed high-confidence MTA and ALKBH10B targets. Hypomethylated transcripts were determined as those loosing m^{6}A in both deficient mutants. Gene functional ontology (GO enrichment) was performed on transcripts with significant m^{6}A peaks using DAVID tools set at default parameters (Huang da et al. 2009). Background genes for each GO enrichment analysis were set to all transcripts detected across all conditions deemed to contain significant m^{6}A peaks using MACS2. To determine differentially methylated peaks between genotypes and conditions, the m^{6}A site differential algorithm was used (Meng et al. 2013). Transcripts with ≥1.5 FC decrease in m^{6}A signal in both *mta* and *35S:ALKBH10B* compared to in Col-0 and with a $P < 0.05$ were used for subsequent analysis. Motif analysis was carried out using HOMER (version 4.7; http://homer.ucsd.edu/homer), 6 nucleotide length.

Measurement of mRNA cleavage and stability through proportion uncapped metric

RNA-seq and GMUCT-seq 50 nt single-end raw reads were trimmed to remove adapter sequences using Cutadapt (Martin 2011). Trimmed reads were aligned to the *Arabidopsis* reference genome using STAR as described above (Dobin et al. 2013). HTSeq was utilized to determine the number of raw reads mapping to each given transcript using strand-specific parameters (Anders et al. 2015). Mapped reads for each transcript were normalized to total mapped RPM. Proportion uncapped was calculated using the calculated RPM from mRNA-seq and GMUCT-seq libraries as previously described (Anderson et al. 2018). Proportion uncapped was defined as $\log_2$ ratio of normalized GMUCT reads divided by normalized RNA-seq reads for each transcript ($(\log_2[RPM_{GMUCT}/RPM_{RNA-seq}])$). Transcripts with higher proportion uncapped were considered "de-stabilized" *mta* compared Col-0 and before and after flg22 treatment. To determine percent cleaved within m6A peaks, a number of cleavage sites determined through GMUCT were overlapped within significant m^{6}A peaks. Details of all statistical tests used in this study can be found in Supplemental Data Set S5.

Accession numbers

Sequence data from this article can be found in the GenBank/EMBL data libraries under the following accession numbers: AT4G02940, AT3G05680, AT3G54170, AT3G05680, AT1G02120, AT1G06137, AT2G33540, AT2G46400, AT1G 10570, AT4G22330, AT5G67450, AT3G25140, AT1G18590, AT2G22300, AT2G32240, AT2G45220, and AT4G10760.

Author contributions

B.D.G., H.H., and M.C. conceived the work. W.P., A.H.S., J. Bazin, J. Bigeard, M.A-T., and B.D.G. generated and analyzed the data. All authors wrote and revised the manuscript.

Supplemental data

The following materials are available in the online version of this article.

Supplemental Figure S1. Detailed analysis of genotypes used and further phenotyping of immune responses.

Supplemental Figure S2. Transcriptome profile during pathogen stress in m^{6}A-depleted backgrounds.

Supplemental Figure S3. m^{6}A-seq peak calling and reproducibility.

Supplemental Figure S4. m^{6}A-seq peak coverage and transcript profile.

Supplemental Figure S5. Motif analysis in high-confidence m^{6}A peaks across conditions.

Supplemental Figure S6. Changes in m^{6}A enrichment before and after pathogen treatment.

Supplemental Figure S7. Combined analysis of m^{6}A- and mRNA-seq.

Supplemental Figure S8. Analysis of m^{6}A-dependent transcript abundance.

Supplemental Data Set S1. Differentially abundant mRNA-seq transcript annotation.

Supplemental Data Set S2. Differentially methylated transcript annotation.

Supplemental Data Set S3. GMUCT proportion uncapped transcript annotation.

Supplemental Data Set S4. List of all primers used in this study.

Supplemental Data Set S5. Summary of statistical tests used in this study.

Funding

This publication is based upon work supported by grants from the National Science Foundation (United States) (IOS-2023310 and IOS-1849708) to B.D.G. Additionally, this work was supported by grants from the King Abdullah University of Science and Technology (KAUST) to H.H., No. BAS/1/1062-01-01, and by grants of the KAUST International Program OCRF-2014-CRG4 to H.H. and M.C. M.C. benefits from the support of Universitie Paris-Saclay (Saclay Plant Sciences-SPS) (ANR-17-EUR-0007). The funders had no role in the study design, data collection and analysis, decision to publish, or preparation of the manuscript.

Conflicts of interest. The authors declare no conflicts or interest or competing interests.

Data availability

Sequencing data associated with the mRNA-seq, m^{6}A-seq, and GMUCT-seq have been deposited in GEO (GEO accession: GSE171536).

References

Almeida Trapp M, De Souza GD, Rodrigues-Filho E, Boland W, Mithöfer A. Validated method for phytohormone quantification in

plants. Front Plant Sci. 2014:**5**(1):417. https://doi.org/10.3389/fpls.2014.00417

Alvarado-Marchena L, Marquez-Molins J, Martinez-Perez M, Aparicio F, Pallás V. Mapping of functional subdomains in the at ALKBH9B m6A-demethylase required for its binding to the viral RNA and to the coat protein of alfalfa mosaic virus. Front Plant Sci. 2021:**12**(1):701683. https://doi.org/10.3389/fpls.2021.701683

Anders M, Chelysheva I, Goebel I, Trenkner T, Zhou J, Mao Y, Verzini S, Qian S-B, Ignatova Z. Dynamic m6A methylation facilitates mRNA triaging to stress granules. Life Sci Alliance. 2018:**1**(4):e201800113. https://doi.org/10.26508/lsa.201800113

Anders S, Pyl PT, Huber W. HTSeq—a python framework to work with high-throughput sequencing data. Bioinformatics 2015:**31**(2):166–169. https://doi.org/10.1093/bioinformatics/btu638

Anderson SJ, Kramer MC, Gosai SJ, Yu X, Vandivier LE, Nelson ADL, Anderson ZD, Beilstein MA, Fray RG, Lyons E, et al. N^6-methyladenosine inhibits local ribonucleolytic cleavage to stabilize mRNAs in *Arabidopsis*. Cell Rep. 2018:**25**(5):1146–1157.e3. https://doi.org/10.1016/j.celrep.2018.10.020

Arribas-Hernández L, Bressendorff S, Hansen MH, Poulsen C, Erdmann S, Brodersen P. An m6A-YTH module controls developmental timing and morphogenesis in Arabidopsis. Plant Cell 2018:**30**(5):952–967. https://doi.org/10.1105/tpc.17.00833

Batista PJ, Molinie B, Wang J, Qu K, Zhang J, Li L, Bouley DM, Lujan E, Haddad B, Daneshvar K, et al. m6A RNA modification controls cell fate transition in mammalian embryonic stem cells. Cell Stem Cell 2014:**15**(6):707–719. https://doi.org/10.1016/j.stem.2014.09.019

Bazin J, Romero N, Rigo R, Charon C, Blein T, Ariel F, Crespi M. Nuclear speckle RNA binding proteins remodel alternative splicing and the non-coding *Arabidopsis* transcriptome to regulate a cross-talk between auxin and immune responses. Front Plant Sci. 2018:**9**(1):1209. https://doi.org/10.3389/fpls.2018.01209

Berens ML, Berry HM, Mine A, Argueso CT, Tsuda K. Evolution of hormone signaling networks in plant defense. Annu Rev Phytopathol. 2017:**55**(1):401–425. https://doi.org/10.1146/annurev-phyto-080516-035544

Bethke G, Grundman RE, Sreekanta S, Truman W, Katagiri F, Glazebrook J. *Arabidopsis* PECTIN METHYLESTERASEs contribute to immunity against *Pseudomonas syringae*. Plant Physiol. 2014:**164**(2):1093–1107. https://doi.org/10.1104/pp.113.227637

Bhat SS, Bielewicz D, Gulanicz T, Bodi Z, Yu X, Anderson SJ, Szewc L, Bajczyk M, Dolata J, Grzelak N, et al. mRNA adenosine methylase (MTA) deposits m6A on pri-miRNAs to modulate miRNA biogenesis in *Arabidopsis thaliana*. Proc Natl Acad Sci U S A. 2020:**117**(35):21785–21795. https://doi.org/10.1073/pnas.2003733117

Bigeard J, Colcombet J, Hirt H. Signaling mechanisms in pattern-triggered immunity (PTI). Mol Plant. 2015:**8**(4):521–539. https://doi.org/10.1016/j.molp.2014.12.022

Birkenbihl RP, Liu S, Somssich IE. Transcriptional events defining plant immune responses. Curr Opin Plant Biol. 2017:**38**(1):1–9. https://doi.org/10.1016/j.pbi.2017.04.004

Bodi Z, Zhong S, Mehra S, Song J, Graham N, Li H, May S, Fray RG. Adenosine methylation in *Arabidopsis* mRNA is associated with the 3′ end and reduced levels cause developmental defects. Front Plant Sci. 2012:**3**(1):48. https://doi.org/10.3389/fpls.2012.00048

Choi J, Ieong K-W, Demirci H, Chen J, Petrov A, Prabhakar A, O'Leary SE, Dominissini D, Rechavi G, Soltis SM, et al. N(6)-methyladenosine in mRNA disrupts tRNA selection and translation-elongation dynamics. Nat Struct Mol Biol. 2016:**23**(2):110–115. https://doi.org/10.1038/nsmb.3148

Del Corpo D, Fullone MR, Miele R, Lafond M, Pontiggia D, Grisel S, Kieffer-Jaquinod S, Giardina T, Bellincampi D, Lionetti V. AtPME17 is a functional *Arabidopsis thaliana* pectin methylesterase regulated by its PRO region that triggers PME activity in the resistance to *Botrytis cinerea*. Mol Plant Pathol. 2020:**21**(12):1620–1633. https://doi.org/10.1111/mpp.13002

Denoux C, Galletti R, Mammarella N, Gopalan S, Werck D, De Lorenzo G, Ferrari S, Ausubel FM, Dewdney J. Activation of defense response pathways by OGs and Flg22 elicitors in *Arabidopsis* seedlings. Mol Plant. 2008:**1**(3):423–445. https://doi.org/10.1093/mp/ssn019

Dobin A, Davis CA, Schlesinger F, Drenkow J, Zaleski C, Jha S, Batut P, Chaisson M, Gingeras TR. STAR: ultrafast universal RNA-seq aligner. Bioinformatics 2013:**29**(1):15–21. https://doi.org/10.1093/bioinformatics/bts635

Dobin A, Gingeras TR. Mapping RNA-seq reads with STAR. Curr Protoc Bioinforma. 2015:**51**(1):11.14.1–11.14.19. https://doi.org/10.1002/0471250953.bi1114s51

Dominissini D, Moshitch-Moshkovitz S, Salmon-Divon M, Amariglio N, Rechavi G. Transcriptome-wide mapping of N(6)-methyladenosine by m(6)A-seq based on immunocapturing and massively parallel sequencing. Nat Protoc. 2013:**8**(1):176–189. https://doi.org/10.1038/nprot.2012.148

Dominissini D, Moshitch-Moshkovitz S, Schwartz S, Salmon-Divon M, Ungar L, Osenberg S, Cesarkas K, Jacob-Hirsch J, Amariglio N, Kupiec M, et al. Topology of the human and mouse m6A RNA methylomes revealed by m6A-seq. Nature. 2012:**485**(7397):201–206. https://doi.org/10.1038/nature11112

Dong X, Mindrinos M, Davis KR, Ausubel FM. Induction of *Arabidopsis* defense genes by virulent and avirulent *Pseudomonas syringae* strains and by a cloned avirulence gene. Plant Cell 1991:**3**(1):61–72. https://doi.org/10.1105/tpc.3.1.61

Duan H-C, Wei L-H, Zhang C, Wang Y, Chen L, Lu Z, Chen PR, He C, Jia G. ALKBH10B Is an RNA N^6-methyladenosine demethylase affecting *Arabidopsis* floral transition. Plant Cell 2017:**29**(12):2995–3011. https://doi.org/10.1105/tpc.16.00912

Engel M, Eggert C, Kaplick PM, Eder M, Röh S, Tietze L, Namendorf C, Arloth J, Weber P, Rex-Haffner M, et al. The role of m6A/m-RNA methylation in stress response regulation. Neuron. 2018:**99**(2):389–403.e9. https://doi.org/10.1016/j.neuron.2018.07.009

Engler C, Youles M, Gruetzner R, Ehnert T-M, Werner S, Jones JD, Patron NJ, Marillonnet S. A golden gate modular cloning toolbox for plants. ACS Synth Biol. 2014:**3**(11):839–843. https://doi.org/10.1021/sb4001504

Farhat DC, Bowler MW, Communie G, Pontier D, Belmudes L, Mas C, Corrao C, Couté Y, Bougdour A, Lagrange T, et al. A plant-like mechanism coupling m6A reading to polyadenylation safeguards transcriptome integrity and developmental gene partitioning in toxoplasma. Elife 2021:**10**(1):e68312. https://doi.org/10.7554/eLife.68312

Felix G, Duran JD, Volko S, Boller T. Plants have a sensitive perception system for the most conserved domain of bacterial flagellin. Plant J. 1999:**18**(3):265–276. https://doi.org/10.1046/j.1365-313X.1999.00265.x

Floris M, Mahgoub H, Lanet E, Robaglia C, Menand B. Post-transcriptional regulation of gene expression in plants during abiotic stress. Int J Mol Sci. 2009:**10**(7):3168–3185. https://doi.org/10.3390/ijms10073168

Govindan G, Sharma B, Li Y-F, Armstrong CD, Merum P, Rohila JS, Gregory BD, Sunkar R. mRNA N^6-methyladenosine is critical for cold tolerance in *Arabidopsis*. Plant J. 2022:**111**(4):1052–1068. https://doi.org/10.1111/tpj.15872

Guo T, Liu C, Meng F, Hu L, Fu X, Yang Z, Wang N, Jiang Q, Zhang X, Ma F. The m6A reader MhYTP2 regulates MdMLO19 mRNA stability and antioxidant genes translation efficiency conferring powdery mildew resistance in apple. Plant Biotechnol J. 2022:**20**(3):511–525. https://doi.org/10.1111/pbi.13733

Haussmann IU, Bodi Z, Sanchez-Moran E, Mongan NP, Archer N, Fray RG, Soller M. m6A potentiates Sxl alternative pre-mRNA splicing for robust *Drosophila* sex determination. Nature 2016:**540**(7632):301–304. https://doi.org/10.1038/nature20577

Huang da W, Sherman BT, Lempicki RA. Systematic and integrative analysis of large gene lists using DAVID bioinformatics resources. Nat Protoc. 2009:**4**(1):44–57. https://doi.org/10.1038/nprot.2008.211

Jones JD, Dangl JL. The plant immune system. Nature 2006:**444**(7117): 323–329. https://doi.org/10.1038/nature05286

Jones DA, Takemoto D. Plant innate immunity—direct and indirect recognition of general and specific pathogen-associated molecules. Curr Opin Immunol. 2004:**16**(1):48–62. https://doi.org/10.1016/j.coi.2003.11.016

Khafif M, Balagué C, Huard-Chauveau C, Roby D. An essential role for the VASt domain of the *Arabidopsis* VAD1 protein in the regulation of defense and cell death in response to pathogens. PLoS One 2017:**12**(7):e0179782. https://doi.org/10.1371/journal.pone.0179782

Kodaira K-S, Qin F, Tran L-S, Maruyama K, Kidokoro S, Fujita Y, Shinozaki K, Yamaguchi-Shinozaki K. *Arabidopsis* Cys2/His2 zinc-finger proteins AZF1 and AZF2 negatively regulate abscisic acid-repressive and auxin-inducible genes under abiotic stress conditions. Plant Physiol. 2011:**157**(2):742–756. https://doi.org/10.1104/pp.111.182683

Lampropoulos A, Sutikovic Z, Wenzl C, Maegele I, Lohmann JU, Forner J. GreenGate—a novel, versatile, and efficient cloning system for plant transgenesis. PLoS One 2013:**8**(12):e83043. https://doi.org/10.1371/journal.pone.0083043

Li F, Cheng C, Cui F, de Oliveira MV, Yu X, Meng X, Intorne AC, Babilonia K, Li M, Li B, et al. Modulation of RNA polymerase II phosphorylation downstream of pathogen perception orchestrates plant immunity. Cell Host Microbe. 2014:**16**(6):748–758. https://doi.org/10.1016/j.chom.2014.10.018

Li N, Han X, Feng D, Yuan D, Huang L-J. Signaling crosstalk between salicylic acid and ethylene/jasmonate in plant defense: do we understand what they are whispering? Int J Mol Sci. 2019:**20**(3):671. https://doi.org/10.3390/ijms20030671

Li Z, Shi J, Yu L, Zhao X, Ran L, Hu D, Song B. N 6-methyl-adenosine level in *Nicotiana tabacum* is associated with tobacco mosaic virus. Virol J. 2018:**15**(1):87. https://doi.org/10.1186/s12985-018-0997-4

Liao Y, Smyth GK, Shi W. Featurecounts: an efficient general purpose program for assigning sequence reads to genomic features. Bioinformatics 2014:**30**(7):923–930. https://doi.org/10.1093/bioinformatics/btt656

Liu Z, Hou S, Rodrigues O, Wang P, Luo D, Munemasa S, Lei J, Liu J, Ortiz-Morea FA, Wang X, et al. Phytocytokine signalling reopens stomata in plant immunity and water loss. Nature 2022:**605**(7909): 332–339. https://doi.org/10.1038/s41586-022-04684-3

Lorrain S, Lin B, Auriac MC, Kroj T, Saindrenan P, Nicole M, Balagué C, Roby D. Vascular associated death1, a novel GRAM domain–containing protein, is a regulator of cell death and defense responses in vascular tissues. Plant Cell 2004:**16**(8):2217–2232. https://doi.org/10.1105/tpc.104.022038

Love MI, Huber W, Anders S. Moderated estimation of fold change and dispersion for RNA-seq data with DESeq2. Genome Biol. 2014:**15**(12):550. https://doi.org/10.1186/s13059-014-0550-8

Luo J-H, Wang Y, Wang M, Zhang L-Y, Peng H-R, Zhou Y-Y, Jia G-F, He Y. Natural variation in RNA m6A methylation and its relationship with translational status. Plant Physiol. 2020:**182**(1):332–344. https://doi.org/10.1104/pp.19.00987

Mao Y, Dong L, Liu X-M, Guo J, Ma H, Shen B, Qian S-B. M6a in mRNA coding regions promotes translation via the RNA helicase-containing YTHDC2. Nat Commun. 2019:**10**(1):5332. https://doi.org/10.1038/s41467-019-13317-9

Mao X, Hou N, Liu Z, He J. Profiling of N^6-methyladenosine (m6A) modification landscape in response to drought stress in apple (*Malus prunifolia* (Willd. Borkh). Plants (Basel) 2022:**11**(1):103. https://doi.org/10.3390/plants11010103

Martin M. Cutadapt removes adapter sequences from high-throughput sequencing reads. EMBnet J. 2011:**17**(1):10–12. https://doi.org/10.14806/ej.17.1.200

Martínez-Pérez M, Aparicio F, López-Gresa MP, Bellés JM, Sánchez-Navarro JA, Pallás V. *Arabidopsis* m6A demethylase activity modulates viral infection of a plant virus and the m6A abundance in its genomic RNAs. Proc Natl Acad Sci U S A. 2017:**114**(40):10755–10760. https://doi.org/10.1073/pnas.1703139114

Meng J, Cui X, Liu H, Zhang L, Zhang S, Rao MK, Chen Y, Huang Y. Unveiling the dynamics in RNA epigenetic regulations. In 2013 IEEE International Conference on Bioinformatics and Biomedicine. 2013:139–144. https://doi.org/10.1109/BIBM.2013.6732477

Meyer KD, Saletore Y, Zumbo P, Elemento O, Mason CE, Jaffrey SR. Comprehensive analysis of mRNA methylation reveals enrichment in 3′ UTRs and near stop codons. Cell 2012:**149**(7):1635–1646. https://doi.org/10.1016/j.cell.2012.05.003

Myers RJ, Fichman Y, Zandalinas SI, Mittler R. Jasmonic acid and salicylic acid modulate systemic reactive oxygen species signaling during stress responses. Plant Physiol. 2023:**191**(2):862–873. https://doi.org/10.1093/plphys/kiac449

Nishimura MT, Stein M, Hou B-H, Vogel JP, Edwards H, Somerville SC. Loss of a callose synthase results in salicylic acid-dependent disease resistance. Science 2003:**301**(5635):969–972. https://doi.org/10.1126/science.1086716

Parker MT, Knop K, Sherwood AV, Schurch NJ, Mackinnon K, Gould PD, Hall AJ, Barton GJ, Simpson GG. Nanopore direct RNA sequencing maps the complexity of *Arabidopsis* mRNA processing and m6A modification. Elife 2020:**9**(1):e49658. https://doi.org/10.7554/eLife.49658

Penninckx IA, Thomma BP, Buchala A, Métraux JP, Broekaert WF. Concomitant activation of jasmonate and ethylene response pathways is required for induction of a plant defensin gene in *Arabidopsis*. Plant Cell 1998:**10**(12):2103–2113. https://doi.org/10.1105/tpc.10.12.2103

Prall W, Ganguly DR, Gregory BD. The covalent nucleotide modifications within plant mRNAs: what we know, how we find them, and what should be done in the future. Plant Cell 2023:**35**(6): 1801–1816. https://doi.org/10.1093/plcell/koad044

Ranf S, Eschen-Lippold L, Pecher P, Lee J, Scheel D. Interplay between calcium signalling and early signalling elements during defence responses to microbe- or damage-associated molecular patterns. Plant J. 2011:**68**(1):100–113. https://doi.org/10.1111/j.1365-313X.2011.04671.x

Rayapuram N, Jarad M, Alhoraibi HM, Bigeard J, Abulfaraj AA, Völz R, Mariappan KG, Almeida-Trapp M, Schlöffel M, Lastrucci E, et al. Chromatin phosphoproteomics unravels a function for AT-hook motif nuclear localized protein AHL13 in PAMP-triggered immunity. Proc Natl Acad Sci U S A. 2021:**118**(3):e2004670118. https://doi.org/10.1073/pnas.2004670118

Reichel M, Köster T, Staiger D. Marking RNA: m6A writers, readers, and functions in *Arabidopsis*. J Mol Cell Biol. 2019:**11**(10):899–910. https://doi.org/10.1093/jmcb/mjz085

Rigo R, Bazin JRM, Crespi M, Charon C. Alternative splicing in the regulation of plant–microbe interactions. Plant Cell Physiol. 2019:**60**(9):1906–1916. https://doi.org/10.1093/pcp/pcz086

Roundtree IA, He C. RNA epigenetics—chemical messages for post-transcriptional gene regulation. Curr Opin Chem Biol. 2016:**30**(1): 46–51. https://doi.org/10.1016/j.cbpa.2015.10.024

Růžička K, Zhang Mi, Campilho A, Bodi Z, Kashif M, Saleh M, Eeckhout D, El-Showk S, Li H, Zhong S, et al. Identification of factors required for m6 A mRNA methylation in *Arabidopsis* reveals a role for the conserved E3 ubiquitin ligase HAKAI. New Phytol. 2017:**215**(1):157–172. https://doi.org/10.1111/nph.14586

Schenk PM, Kazan K, Wilson I, Anderson JP, Richmond T, Somerville SC, Manners JM. Coordinated plant defense responses in *Arabidopsis* revealed by microarray analysis. Proc Natl Acad Sci U S A. 2000:**97**(21): 11655–11660. https://doi.org/10.1073/pnas.97.21.11655

Schwartz S, Mumbach MR, Jovanovic M, Wang T, Maciag K, Bushkin GG, Mertins P, Ter-Ovanesyan D, Habib N, Cacchiarelli D, et al. Perturbation of m6A writers reveals two distinct classes of mRNA methylation at internal and 5′ sites. Cell Rep. 2014:**8**(1):284–296. https://doi.org/10.1016/j.celrep.2014.05.048

Scutenaire J, Deragon J-M, Jean V, Benhamed M, Raynaud C, Favory J-J, Merret R, Bousquet-Antonelli C. The YTH domain protein ECT2 is an m6A reader required for normal trichome branching in *Arabidopsis*. Plant Cell 2018:**30**(5):986–1005. https://doi.org/10.1105/tpc.17.00854

Shao Y, Wong CE, Shen L, Yu H. N^6-methyladenosine modification underlies messenger RNA metabolism and plant development. Curr Opin Plant Biol. 2021:**63**(1):102047. https://doi.org/10.1016/j.pbi.2021.102047

Sharma B, Prall W, Bhatia G, Gregory BD. The diversity and functions of plant RNA modifications: what we know and where we go from here. Annu Rev Plant Biol. 2023:**74**(1):53–85. https://doi.org/10.1146/annurev-arplant-071122-085813

Slobodin B, Han R, Calderone V, Vrielink JAFO, Loayza-Puch F, Elkon R, Agami R. Transcription impacts the efficiency of mRNA translation via co-transcriptional N6-adenosine methylation. Cell 2017:**169**(2):326–337.e12. https://doi.org/10.1016/j.cell.2017.03.031

Sorenson RS, Deshotel MJ, Johnson K, Adler FR, Sieburth LE. *Arabidopsis* mRNA decay landscape arises from specialized RNA decay substrates, decapping-mediated feedback, and redundancy. Proc Natl Acad Sci U S A. 2018:**115**(7):E1485–E1494. https://doi.org/10.1073/pnas.1712312115

Tian S, Wu N, Zhang L, Wang X. RNA N^6-methyladenosine modification suppresses replication of rice black streaked dwarf virus and is associated with virus persistence in its insect vector. Mol Plant Pathol. 2021:**22**(9):1070–1081. https://doi.org/10.1111/mpp.13097

Vandivier LE, Campos R, Kuksa PP, Silverman IM, Wang L-S, Gregory BD. Chemical modifications mark alternatively spliced and uncapped messenger RNAs in *Arabidopsis*. Plant Cell 2015:**27**(11):3024–3037. https://doi.org/10.1105/tpc.15.00591

Wang Y, Li X, Fan B, Zhu C, Chen Z. Regulation and function of defense-related callose deposition in plants. Int J Mol Sci. 2021:**22**(5):2393. https://doi.org/10.3390/ijms22052393

Wang Y, Li Y, Toth JI, Petroski MD, Zhang Z, Zhao JC. N^6-methyladenosine modification destabilizes developmental regulators in embryonic stem cells. Nat Cell Biol. 2014:**16**(2):191–198. https://doi.org/10.1038/ncb2902

Wang Z, Li X, Wang X, Liu N, Xu B, Peng Q, Guo Z, Fan B, Zhu C, Chen Z. *Arabidopsis* endoplasmic reticulum-localized UBAC2 proteins interact with PAMP-INDUCED COILED-COIL to regulate pathogen-induced callose deposition and plant immunity. Plant Cell 2019:**31**(1):153–171. https://doi.org/10.1105/tpc.18.00334

Wang X, Lu Z, Gomez A, Hon GC, Yue Y, Han D, Fu Y, Parisien M, Dai Q, Jia G, et al. m6A-dependent regulation of messenger RNA stability. Nature 2014:**505**(7481):117–120. https://doi.org/10.1038/nature12730

Wang X, Zhao BS, Roundtree IA, Lu Z, Han D, Ma H, Weng X, Chen K, Shi H, He C. N^6-methyladenosine modulates messenger RNA translation efficiency. Cell 2015:**161**(6):1388–1399. https://doi.org/10.1016/j.cell.2015.05.014

Wang L, Zhuang H, Fan W, Zhang X, Dong H, Yang H, Cho J. m6A RNA methylation impairs gene expression variability and reproductive thermotolerance in *Arabidopsis*. Genome Biol. 2022:**23**(1):244. https://doi.org/10.1186/s13059-022-02814-8

Wei L-H, Song P, Wang Y, Lu Z, Tang Q, Yu Q, Xiao Y, Zhang X, Duan H-C, Jia G. The m6A reader ECT2 controls trichome morphology by affecting mRNA stability in *Arabidopsis*. Plant Cell 2018:**30**(5):968–985. https://doi.org/10.1105/tpc.17.00934

Wilkinson E, Cui Y-H, He Y-Y. Context-dependent roles of RNA modifications in stress responses and diseases. Int J Mol Sci. 2021:**22**(4):1949. https://doi.org/10.3390/ijms22041949

Willmann MR, Berkowitz ND, Gregory BD. Improved genome-wide mapping of uncapped and cleaved transcripts in eukaryotes—GMUCT 2.0. Methods 2014:**67**(1):64–73. https://doi.org/10.1016/j.ymeth.2013.07.003

Xie M, Sun J, Gong D, Kong Y. The roles of *Arabidopsis* C1-2i subclass of C2H2-type zinc-finger transcription factors. Genes (Basel) 2019:**10**(9):653. https://doi.org/10.3390/genes10090653

Xin X-F, He SY. *Pseudomonas syringae* pv. tomato DC3000: a model pathogen for probing disease susceptibility and hormone signaling in plants. Annu Rev Phytopathol. 2013:**51**(1):473–498. https://doi.org/10.1146/annurev-phyto-082712-102321

Yang D, Xu H, Liu Y, Li M, Ali M, Xu X, Lu G. RNA N^6-methyladenosine responds to low-temperature stress in tomato anthers. Front Plant Sci. 2021:**12**(1):687826. https://doi.org/10.3389/fpls.2021.687826

Yoon K-J, Ringeling FR, Vissers C, Jacob F, Pokrass M, Jimenez-Cyrus D, Su Y, Kim N-S, Zhu Y, Zheng L, et al. Temporal control of mammalian cortical neurogenesis by m6A methylation. Cell 2017:**171**(4):877–889.e17. https://doi.org/10.1016/j.cell.2017.09.003

Yu Q, Liu S, Yu L, Xiao Y, Zhang S, Wang X, Xu Y, Yu H, Li Y, Yang J, et al. RNA Demethylation increases the yield and biomass of rice and potato plants in field trials. Nat Biotechnol. 2021:**39**(12):1581–1588. https://doi.org/10.1038/s41587-021-00982-9

Zhang X, Henriques R, Lin S-S, Niu Q-W, Chua N-H. *Agrobacterium*-mediated transformation of *Arabidopsis thaliana* using the floral dip method. Nat Protoc. 2006:**1**(2):641–646. https://doi.org/10.1038/nprot.2006.97

Zhang J, Lu H, Li X, Li Y, Cui H, Wen C-K, Tang X, Su Z, Zhou J-M. Effector-triggered and pathogen-associated molecular pattern-triggered immunity differentially contribute to basal resistance to *Pseudomonas syringae*. Mol Plant Microbe Interact. 2010:**23**(7):940–948. https://doi.org/10.1094/MPMI-23-7-0940

Zhang T, Wang Z, Hu H, Chen Z, Liu P, Gao S, Zhang F, He L, Jin P, Xu M, et al. Transcriptome-wide N^6-methyladenosine (m6A) profiling of susceptible and resistant wheat varieties reveals the involvement of variety-specific m6A modification involved in virus-host interaction pathways. Front Microbiol. 2021:**12**(1):656302. https://doi.org/10.3389/fmicb.2021.656302

Zhang D, Zhu Z, Gao J, Zhou X, Zhu S, Wang X, Wang X, Ren G, Kuai B. The NPR1-WRKY46-WRKY6 signaling cascade mediates probenazole/salicylic acid-elicited leaf senescence in *Arabidopsis thaliana*. J Integr Plant Biol. 2021:**63**(5):924–936. https://doi.org/10.1111/jipb.13044

Zhang K, Zhuang X, Dong Z, Xu K, Chen X, Liu F, He Z. The dynamics of N6-methyladenine RNA modification in interactions between rice and plant viruses. Genome Biol. 2021:**22**(1):189. https://doi.org/10.1186/s13059-021-02410-2

Zhao BS, Wang X, Beadell AV, Lu Z, Shi H, Kuuspalu A, Ho RK, He C. m6A-dependent maternal mRNA clearance facilitates zebrafish maternal-to-zygotic transition. Nature 2017:**542**(7642):475–478. https://doi.org/10.1038/nature21355

Zheng G, Dahl JA, Niu Y, Fedorcsak P, Huang C-M, Li CJ, Vågbø CB, Shi Y, Wang W-L, Song S-H, et al. ALKBH5 Is a mammalian RNA demethylase that impacts RNA metabolism and mouse fertility. Mol Cell. 2013:**49**(1):18–29. https://doi.org/10.1016/j.molcel.2012.10.015

Zhou KI, Shi H, Lyu R, Wylder AC, Matuszek Ż, Pan JN, He C, Parisien M, Pan T. Regulation of co-transcriptional pre-mRNA splicing by m6A through the low-complexity protein hnRNPG. Mol Cell. 2019:**76**(1):70–81.e9. https://doi.org/10.1016/j.molcel.2019.07.005

Zhou L, Tang R, Li X, Tian S, Li B, Qin G. N^6-methyladenosine RNA modification regulates strawberry fruit ripening in an ABA-dependent manner. Genome Biol. 2021:**22**(1):168. https://doi.org/10.1186/s13059-021-02385-0